EE213. Microscopic Nanocharacterization of Materials
Lecture 11. 2016

Atom Probe Microscopy

Xray and Photon Induced Microscopies

Homework #2: due Thursday, February 25

Deadlines

February 23. final paper topic

March 1, outline of final paper

EE 213. Winter 2016
Homework#2
Due: February 25, 2016
Maximum score = 100

EE213. Homework #2

1. (50pts) Consider the RBS (Rutherford Backscattering) spectrum shown below taken with 2 Mev He+ ions incident normal to the sample. The sample is a thin Si film deposited onto a higher Z substrate. Which peak is the Si and which is the substrate. What is the substrate and how thick is the Si film? Assume the detector is at a 20 degree angle with respect to the incident beam. The vertical scale is in relative counts. Explain clearly your calculations.

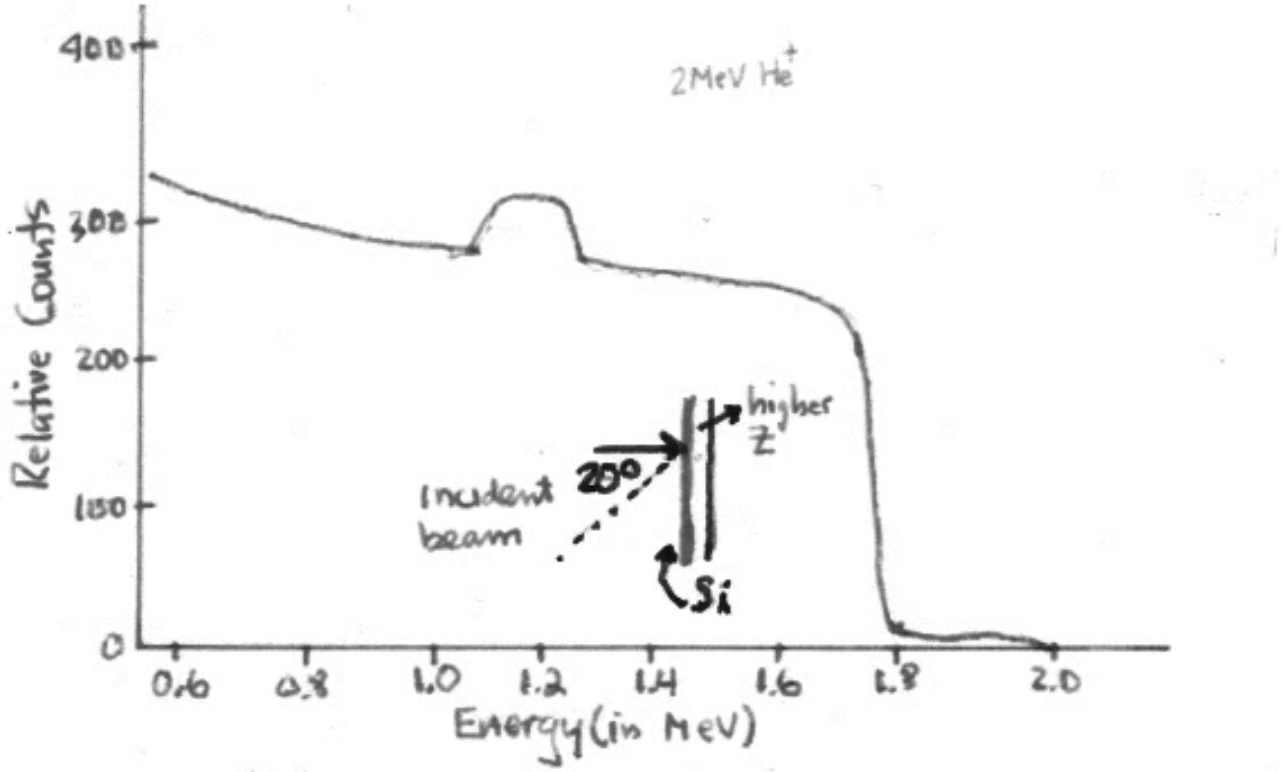

2. (50 pts.) Consider the electron backscattered detector shown below.

A. (25pts.) If the detector electronics allows one to detect signal differences of 1%, can this detector detect a 0.1 atomic number difference at Z= 30? What other information (if any) is needed to make this determination?

B. (25pts.) If we want this detector to be able to filter out all electrons below 1KeV in energy, how thick would the Al metal coating on the detector surface have to be?

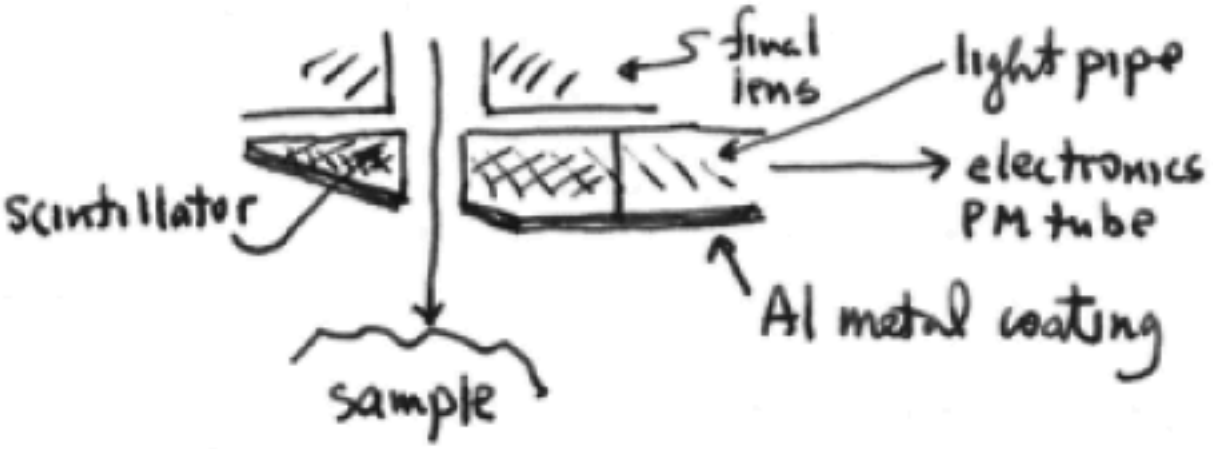

Isolated atom in applied electrc field

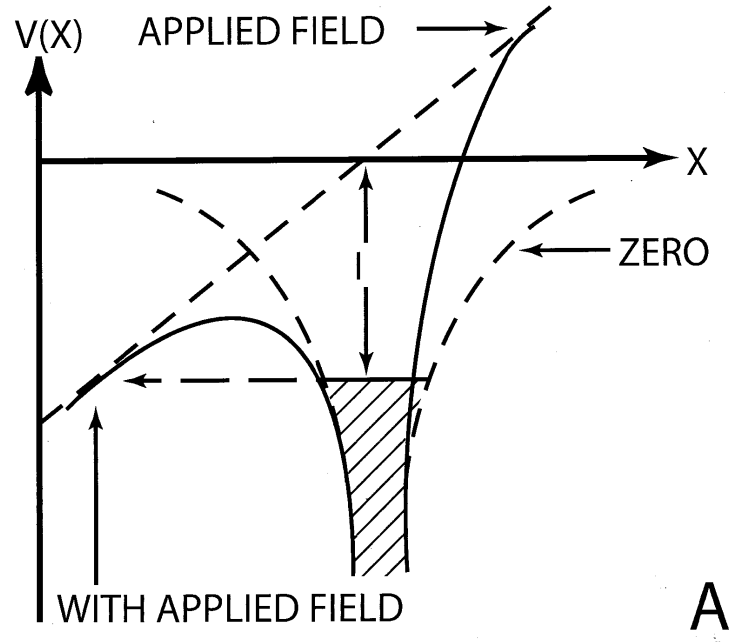

Field Ionization

Atom near a metal surface in an applied electric field

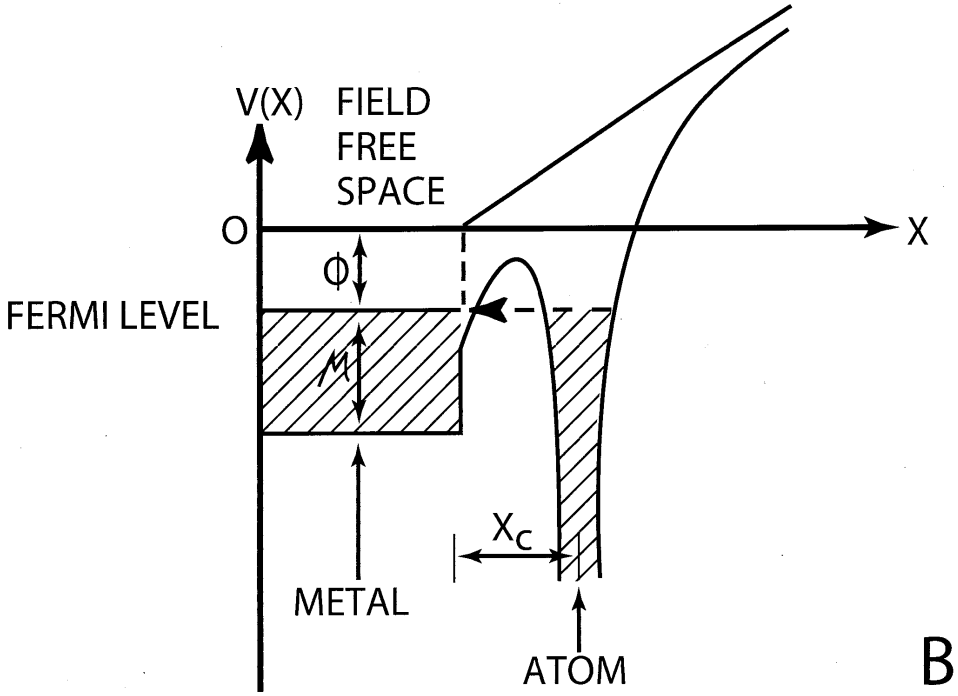

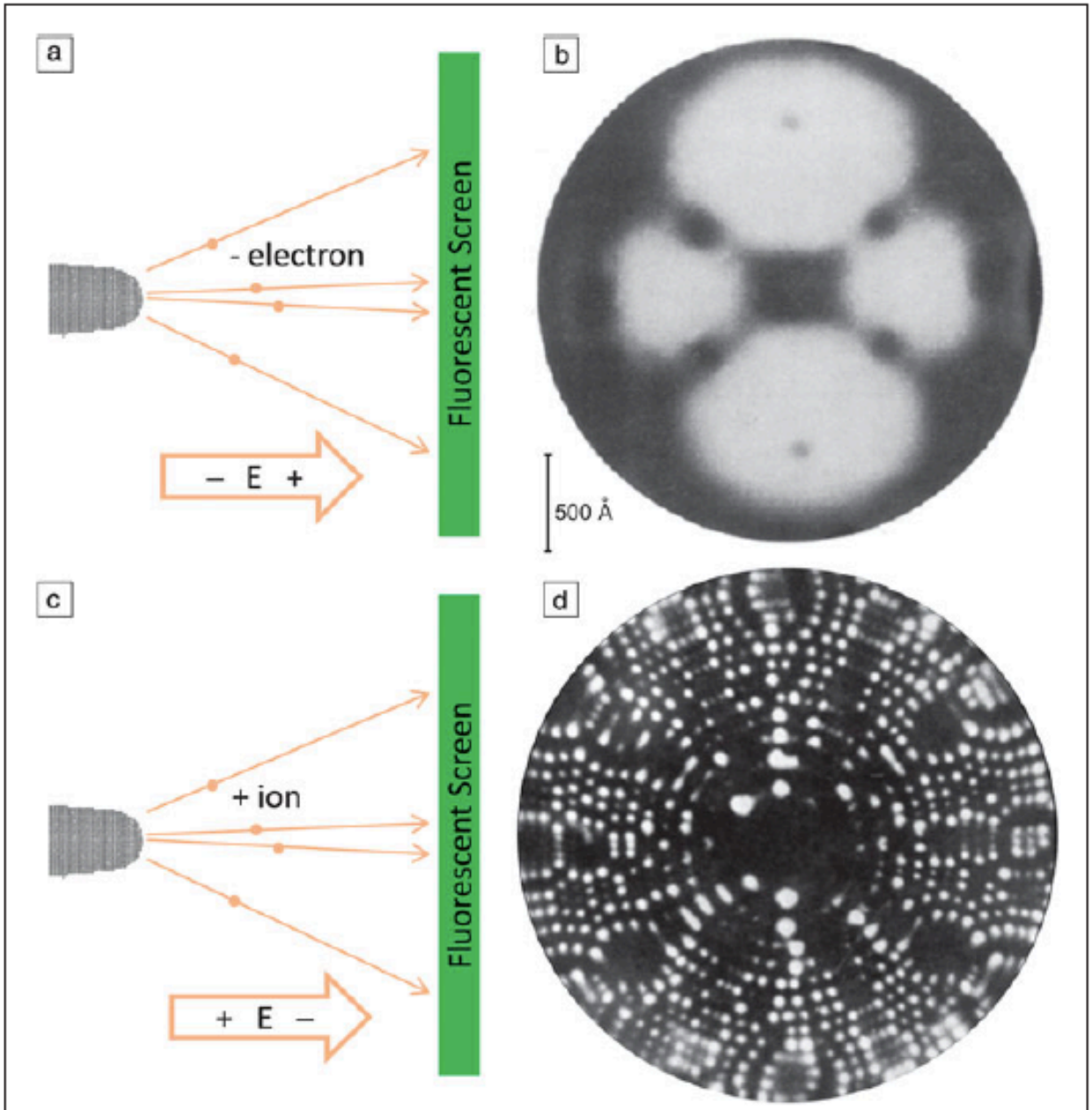

Figure 3. (a) Schematic of the field electron emission microscope (FEEM). (b) FEEM image of <110> tungsten.[14] The twofold symmetry of this pattern is evident. (c) Schematic of the field ion microscope (FIM). (d) FIM image of <110> tungsten.[17,18] The first images of atoms

Field emission

Field ionization

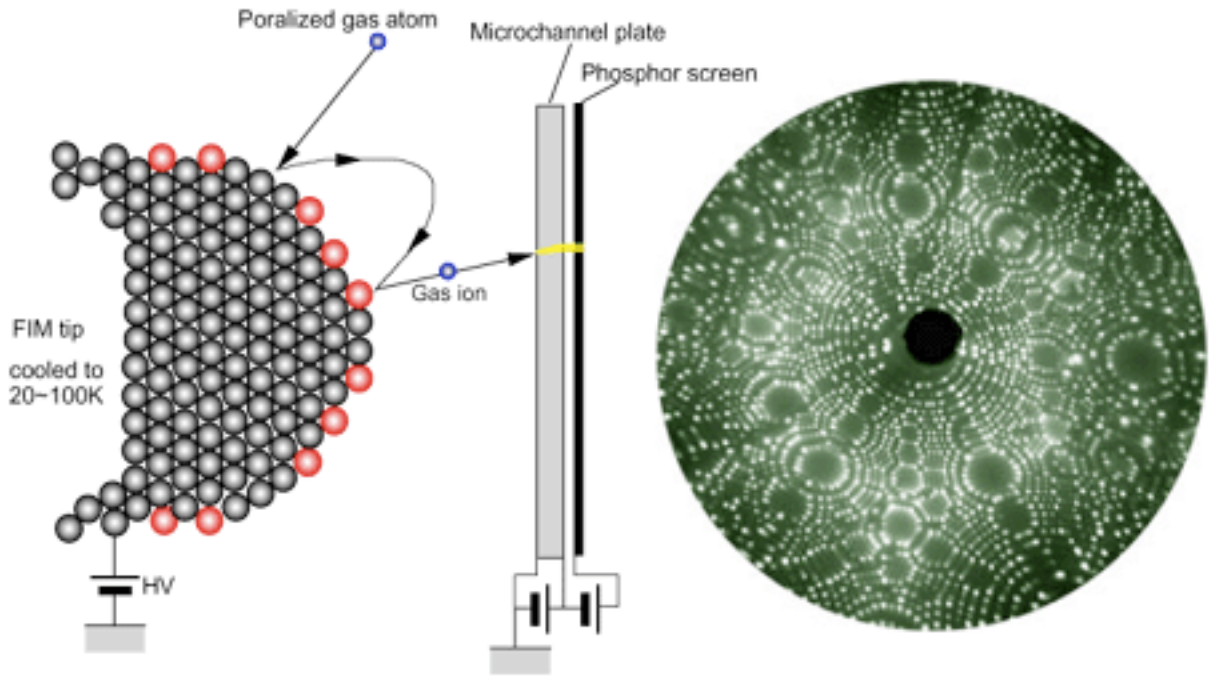

Fig. 1 Principle of field ion microscope (FIM).

Tom Kelly

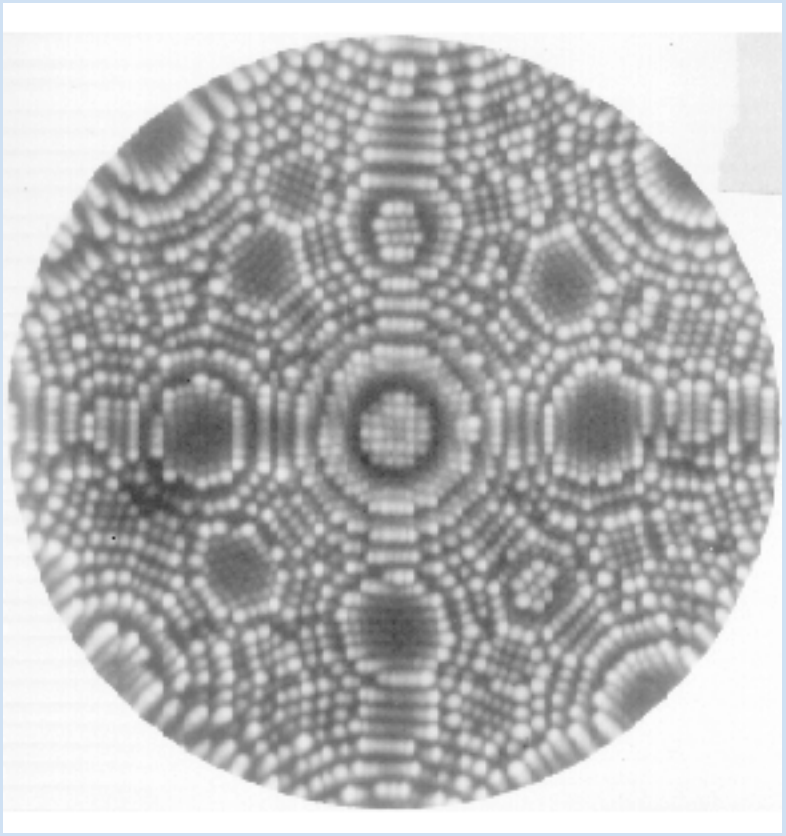

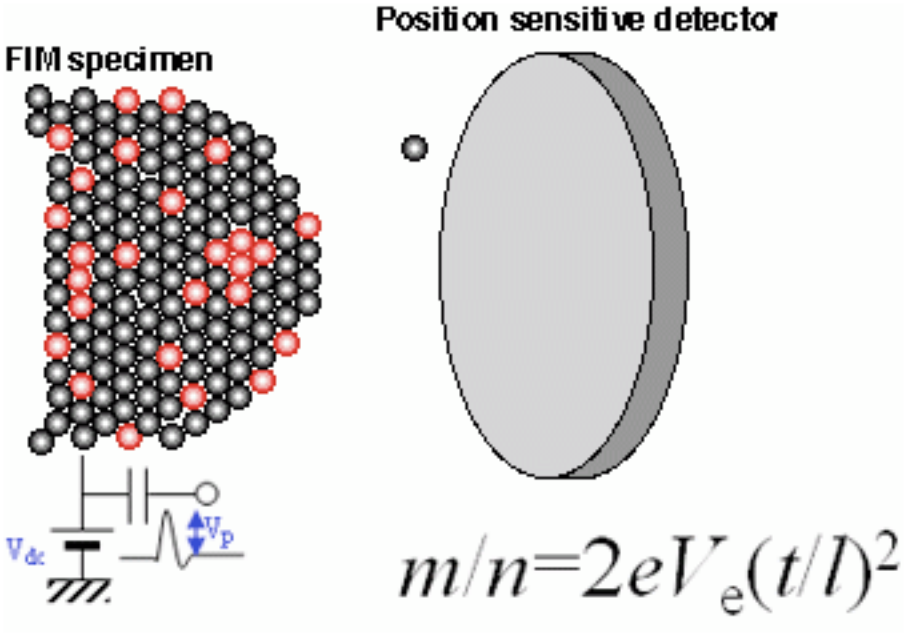

Fig. 1 Schematic illustration of a three dimensional atom probe (3DAP).

Atom Probe Mass Resolution

balance KE ion with PE — (ie, gain in KE = decrease in PE)

$$\therefore \frac{1}{2} m v_{ion}^2 = - neV_T \quad , n = \text{ionization state (ie, 1, 2, etc)}$$

$$\therefore \frac{m}{n} = - \frac{2eV_T}{v_{ion}^2} \quad ; v_{ion} = \frac{R}{t} \leftarrow \text{dist. to screen}$$

$$\therefore \frac{m}{n} = -2eV_T \left(\frac{t}{R}\right)^2$$

$$t^2 = \frac{m}{n}\left(\frac{R^2}{2eV_T}\right)$$

$$\left(\frac{\Delta m}{m}\right)^2 \cong \left(\frac{\Delta V}{V_T}\right)^2 + \left(2\frac{\Delta t}{t}\right)^2 \quad \left(\text{assume } \frac{\Delta R}{R} \to 0\right)$$

$$\boxed{\left(\frac{\Delta m}{m}\right)^2 \cong \left(\frac{\Delta V}{V_T}\right)^2 + \left(\frac{\Delta t}{R}\sqrt{\frac{V_T}{\frac{1}{2e}\frac{m}{n}}}\right)^2}$$

$\Delta V \sim .025 V_{pulse}$ to pull off ions.

$V_{pulse} \sim \frac{1}{5} V_T$

$\Delta t \sim ns$

can get $\frac{\Delta m}{m} \sim 10^{-3} - 10^{-4}$

from Kelly et al. (1996)

R = l from before.
Distance to screen

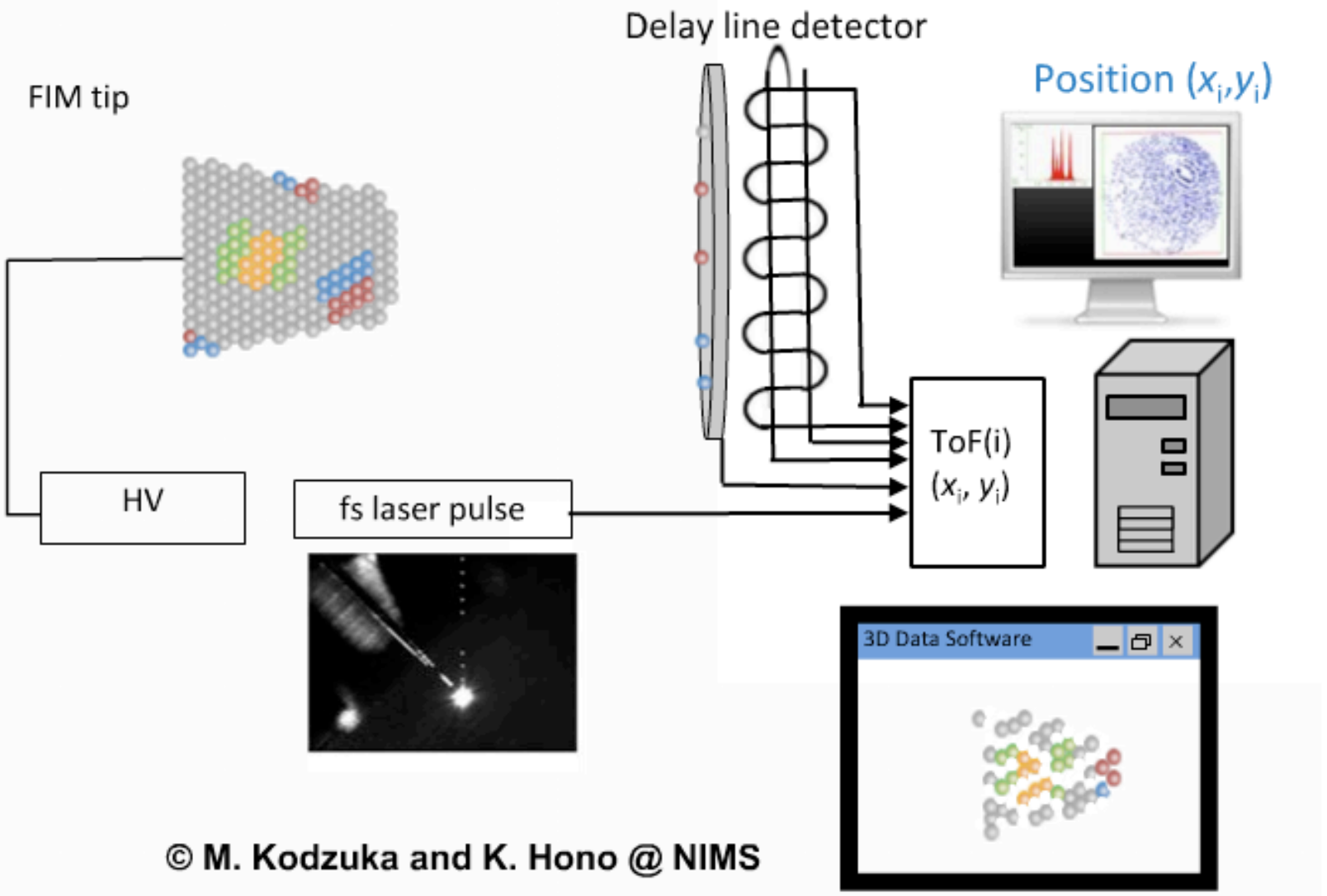
Delay line detector
Position (x_i,y_i)
FIM tip
HV
fs laser pulse
ToF(i)
(x_i, y_i)
3D Data Software
© M. Kodzuka and K. Hono @ NIMS

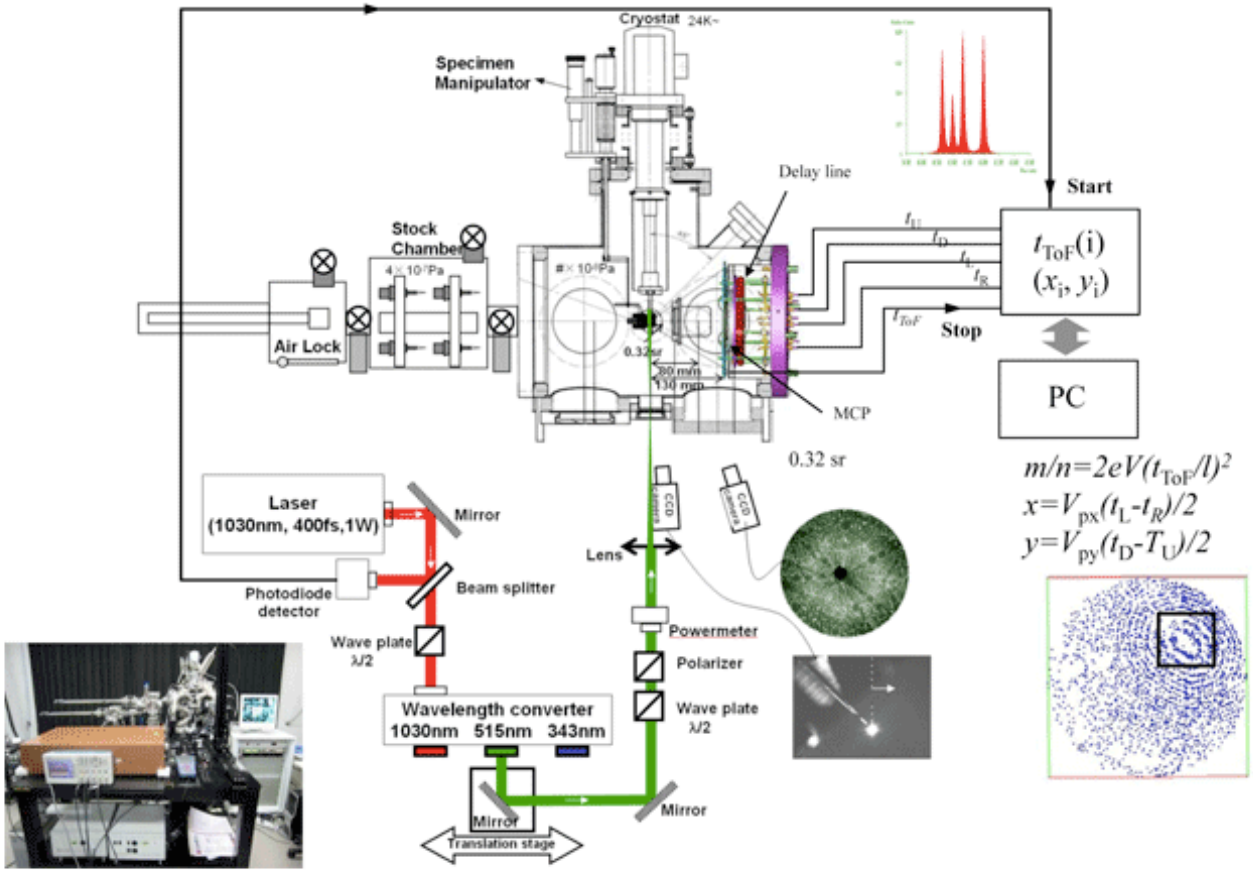

Fig. 2 Schematic illustration of the laser assisted wide angle 3D atom probe at NIMS

T.F.Kelley &M.K.Miller.Rev. Sci.Instr. 78(2007).031101

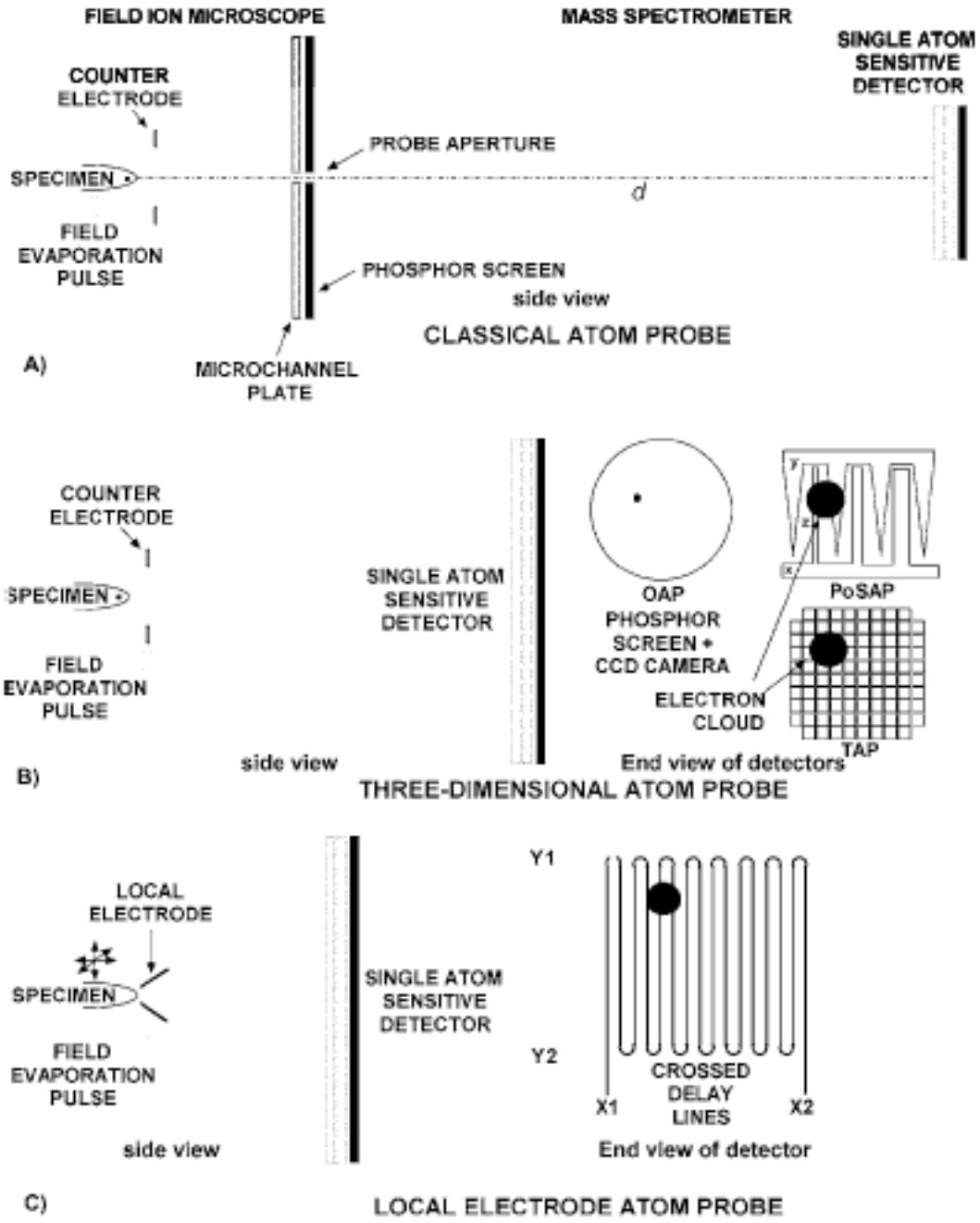

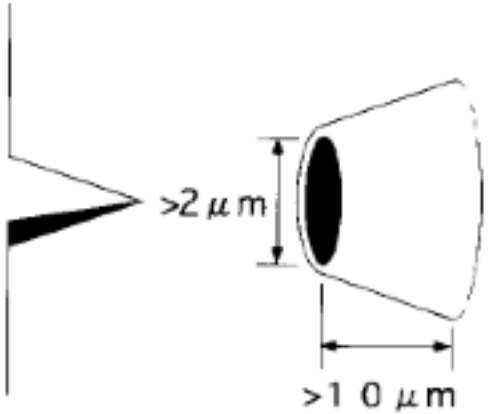

Fig 2 Schematics of the extraction electrode and a tip formed by grooving

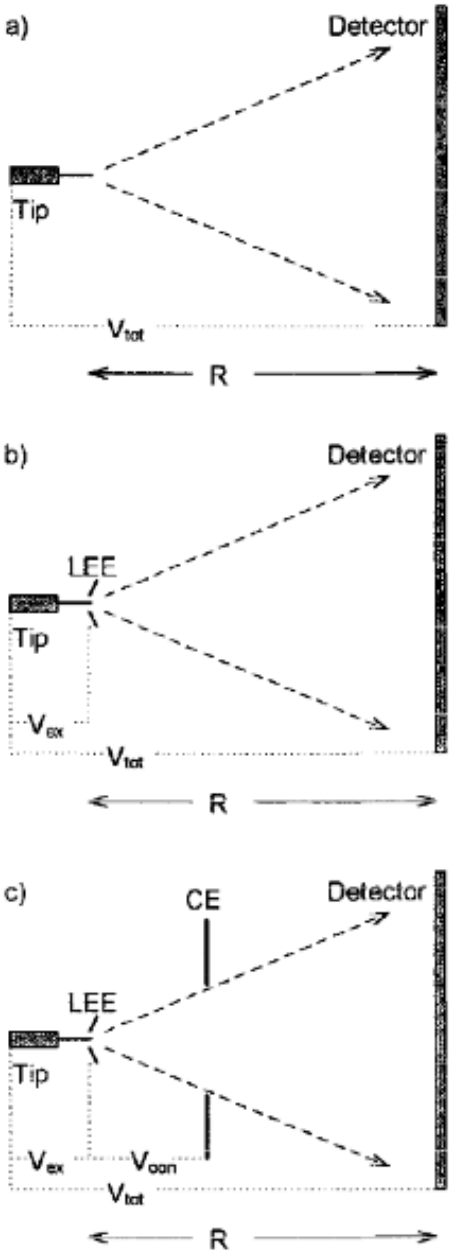

Fig. 2. Schematic illustration of the potentials associated with (a) a conventional atom probe or REAP, (b) a LEAP with a local extraction electrode (LEE), and (c) a LEAP with a separate control electrode (CE).

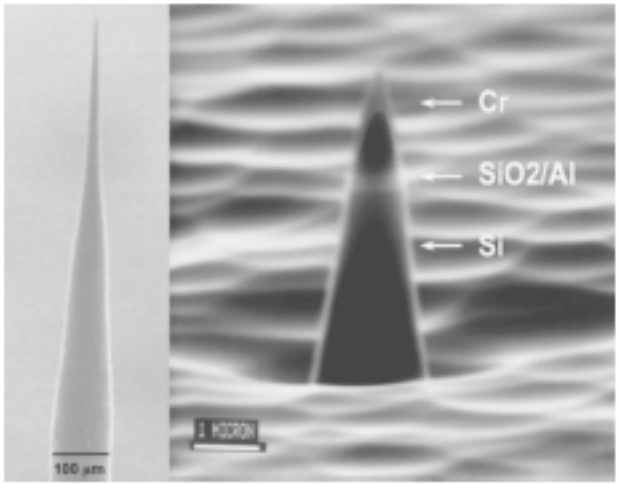

FIG. 3. (a) Scanning electron microscopy (SEM) image of an electropolished specimen of an aluminum alloy. (b) Microtip specimen of a multilayer $Al/SiO_2/Si$ structure fabricated by broad ion beam milling with a diamond mask particle (Ref. 83). Cr was added to the basic structure as a control layer to aid in finding the original layers.

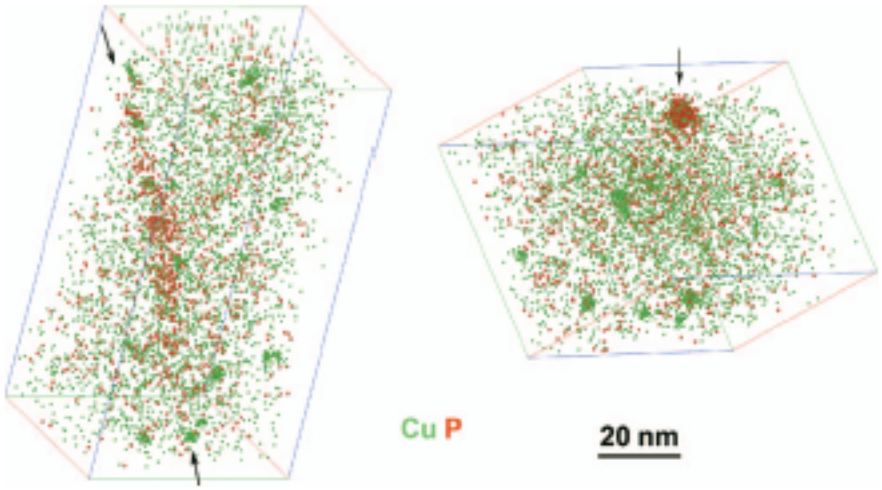

FIG. 6. (Color) Copper (green) and phosphorus (red) atom distribution in a neutron-irradiated (fluence= 1.3×10^{23} n m^{-2} [$E>1$ MeV]) Fe-0.1% Cu, 1.6% Mn, 1.6% Ni model pressure-vessel steel. A high number density of ~3-nm-diameter copper-enriched precipitates and a phosphorus-decorated dislocation are evident. The image on the right is a view along the dislocation that is visible in the left image between the arrows. The arrow in the right image points toward the precipitates that are visible on the dislocation. Specimen is courtesy of Professor G. R. Odette, University of California—Santa Barbara.

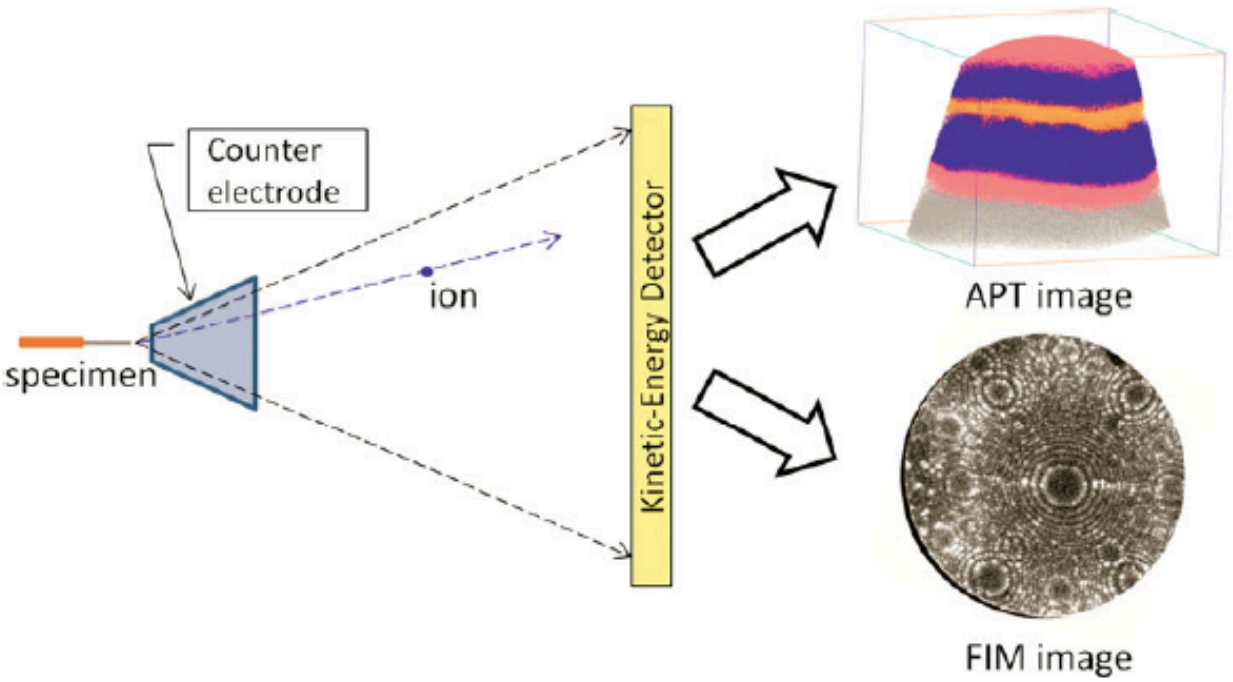

Figure 3. Geometry of kinetic-energy atom probe (Kelly, 2011), an atom probe with kinetic energy discrimination. The detector would be placed close to the specimen to maximize solid angle and data collection rate. Mass resolving power would be diminished by the short flight times, but peak discrimination would be enhanced significantly overall by the augmentation of time-of-flight spectroscopy with kinetic energy information.

From T.F Kelly et.al. Microscopy and Microanalysis. 19.(2013), 662-664.

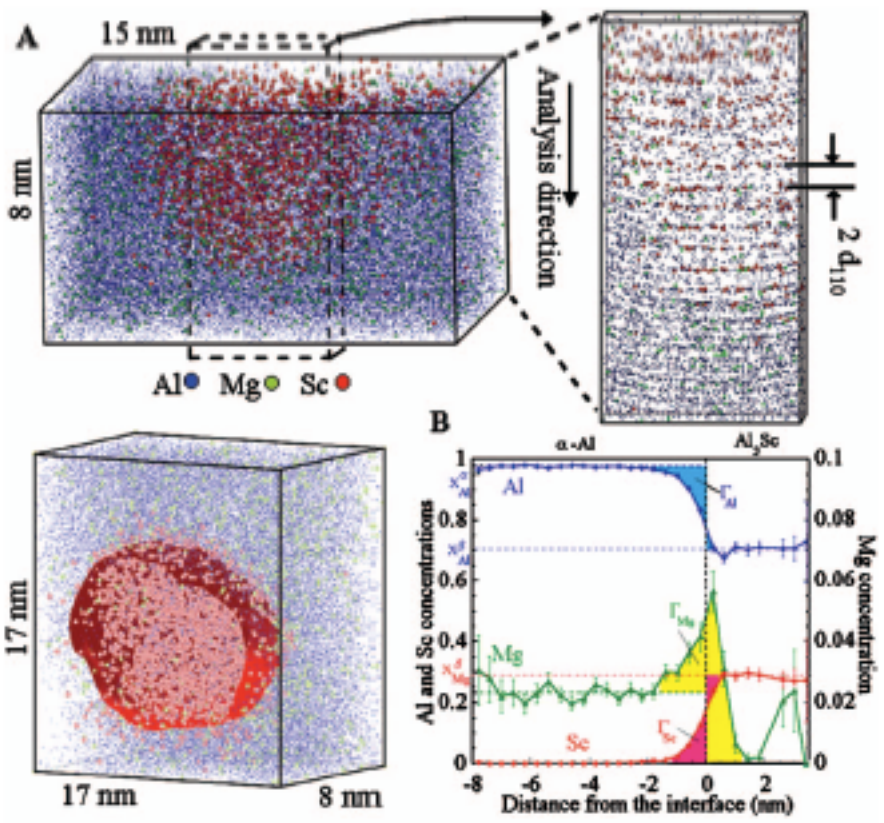

FIG. 11. (Color) APT evaluation of segregation of Mg to an Al_3Sc/Al interface. (a) Image of a precipitate with an isoconcentration surface drawn at 18 at. % Sc. (b) Composition profile derived from a proximity histogram (Ref. 130) which shows the interfacial excesses of Al, Mg, and Sc measured by APT.

Review References for Atom Probe Microscopy

T.F. Kelly, Microscopy and Microanalysis.17. (2011).1-14.

T.F Kelly et.al. Microscopy and Microanalysis. 19. (2013),662-664.

T.F. Kelly and M.K. Miller, Rev. Sci. Instruments.78 (2007).031101.

G. Smith and M. Ruhle. Advances In Analysis of Materials.”European Whie Book on Fundamental Research in Materials Science.(2000) Chap.7.5. “3D Atom Probe”Review

Ionizing Radiation Probes

Electrons

Ions

Xrays

Interactions

prob, $P = \sigma n \, dx$

$$dJ = -JP = -J\sigma n \, dx$$

$$\int_0^x \frac{dJ}{J} = -\int_0^x \sigma n \, dx$$

$$J(x)/J(0) = e^{-n\sigma \cdot x}$$

$n\sigma \cdot x \rightarrow \Lambda = \frac{1}{n\sigma}$, mean free path

mfp = avg. dist. between interactions

Absorption coefficent is inverse of MFP/

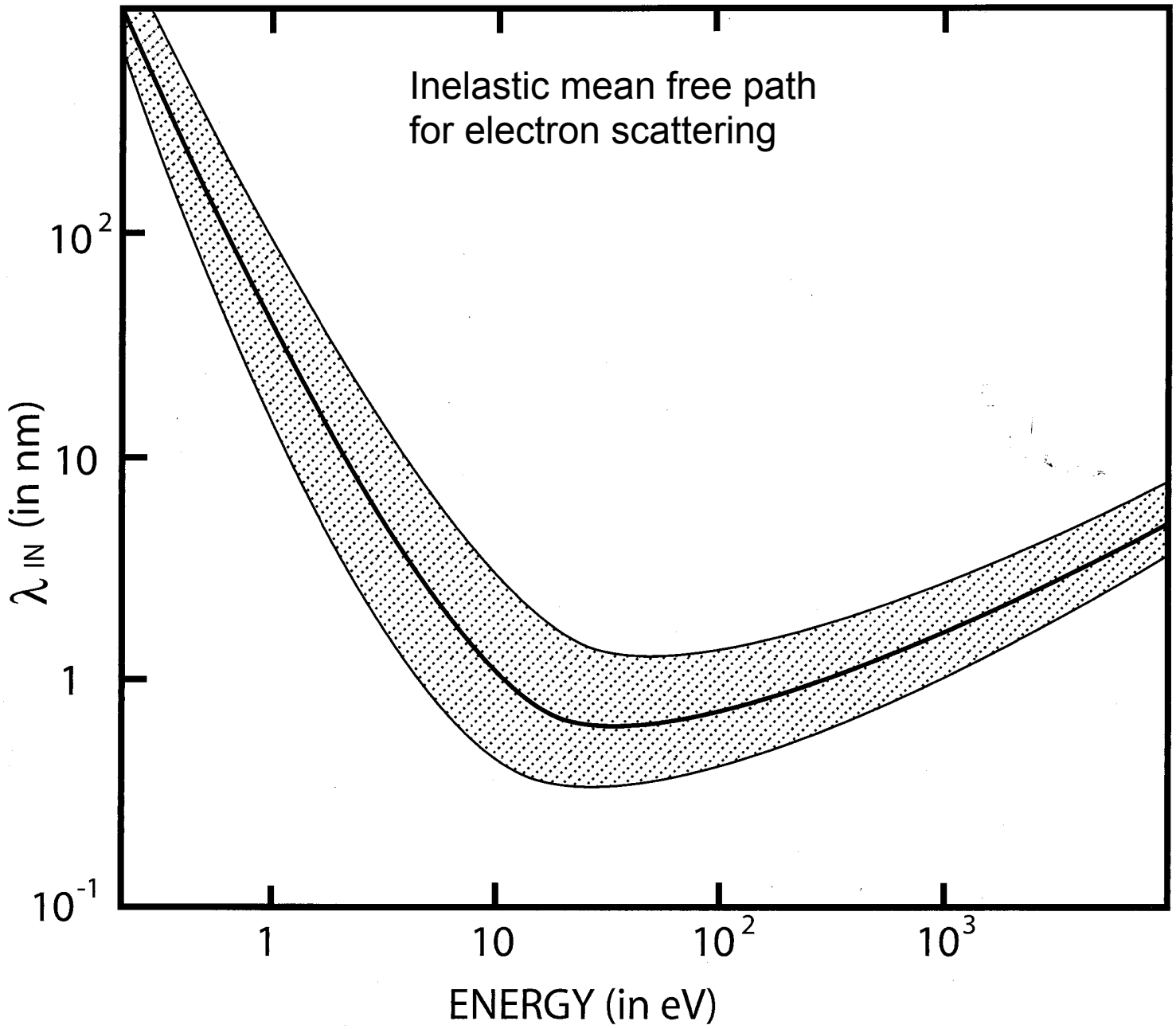

From Seah and Dench, 1979. Surf. and Interface Anal.1.36

Light–matter interaction

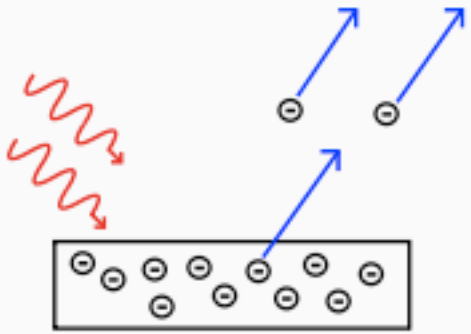

Low-energy phenomena:
Photoelectric effect

Mid-energy phenomena:
Compton scattering

High-energy phenomena:
Pair production

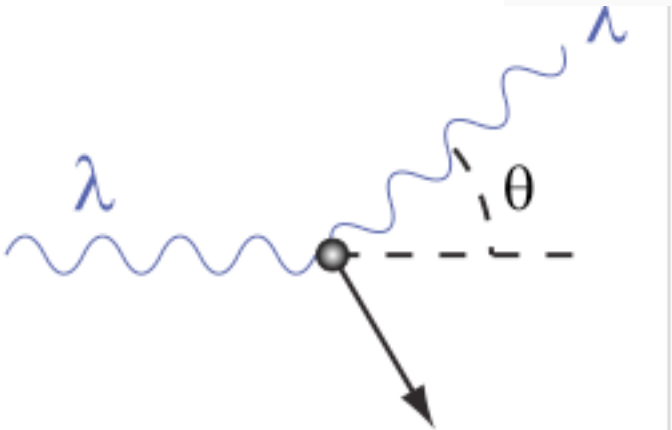

A photon of wavelength λ comes in from the left, collides with a target at rest, and a new photon of wavelength λ' emerges at an angle θ.

$$\lambda' - \lambda = \frac{h}{m_e c}(1 - \cos\theta),$$

From Brodie and Muray, The Physics of Micro/Nanofabrication

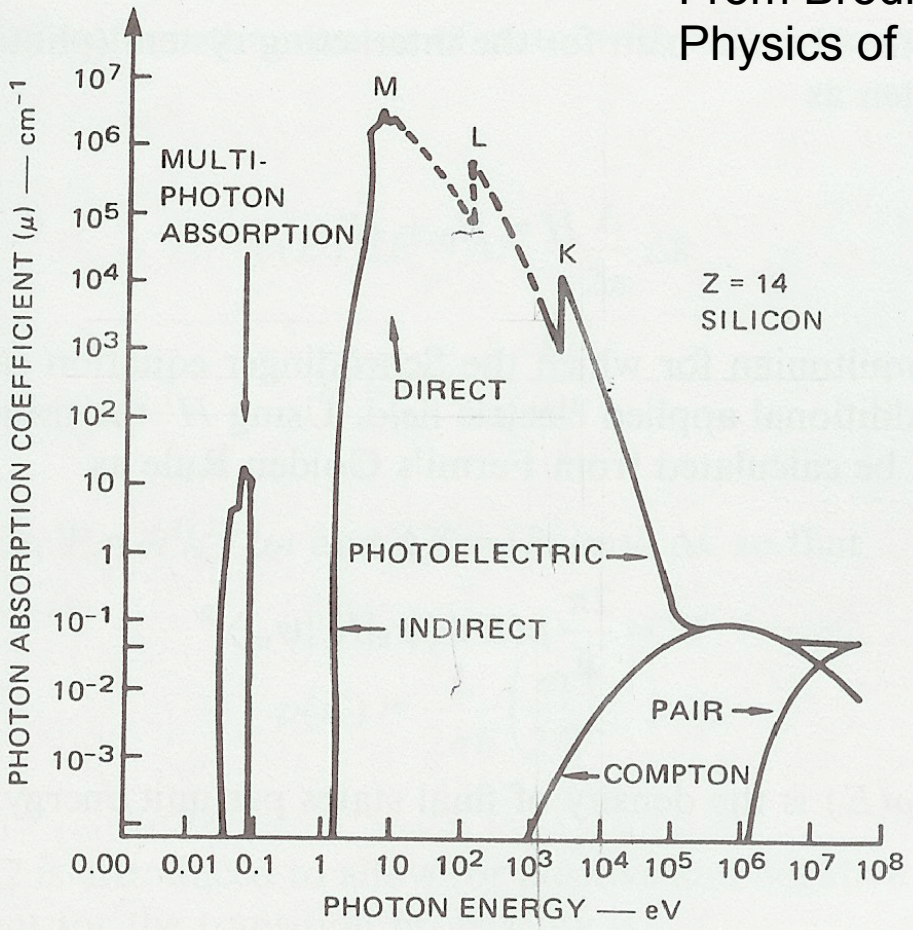

FIGURE 2.100. X-ray absorption coefficient as a function of X-ray energy.

2.9.1.2. Photoelectric Effect. In the photon energy range of 1–50 keV used in microscience, the most important photon interaction is the photoelectric effect. The transmitted X-ray intensity follows an exponential attenuation law expressed as

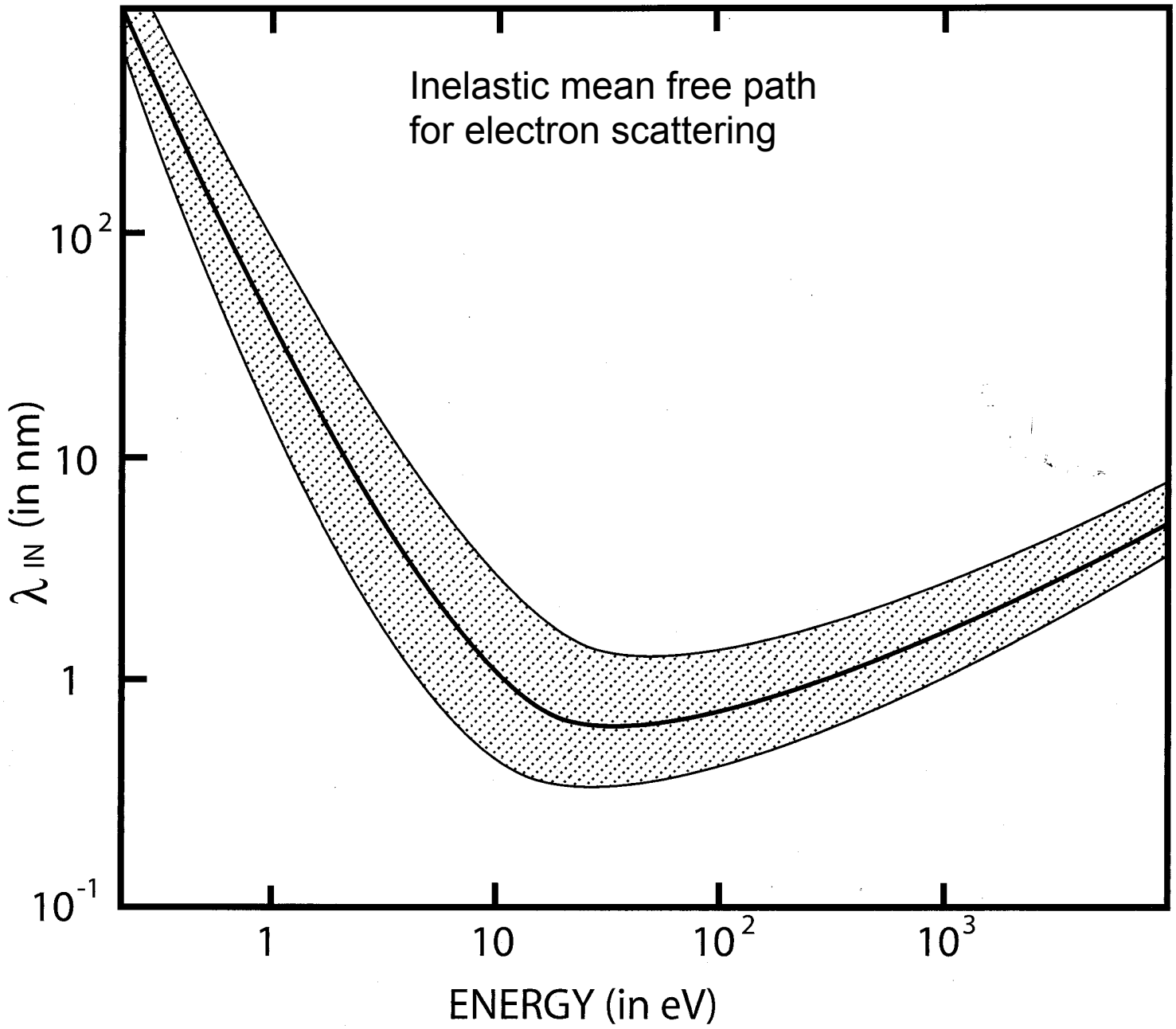

From Seah and Dench, 1979. Surf. and Interface Anal.1.36

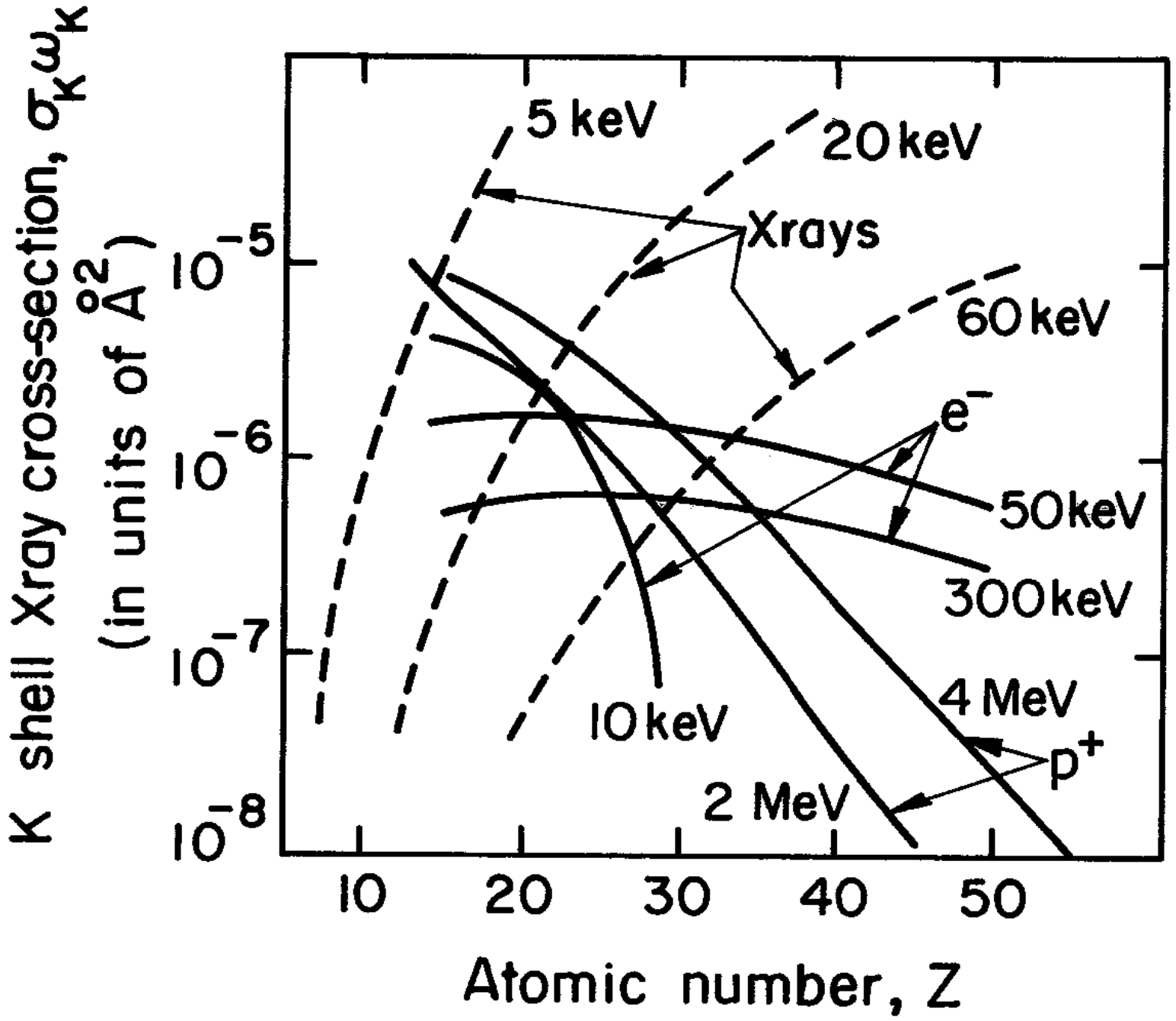
K shell Xray cross-section, $\sigma_K \omega_K$
(in units of $\AA^2$)
10^{-5}
10^{-6}
10^{-7}
10^{-8}
10
20
30
40
50
Atomic number, Z
5 keV
20 keV
Xrays
60 keV
e^-
50 keV
300 keV
4 MeV
p^+
2 MeV
10 keV

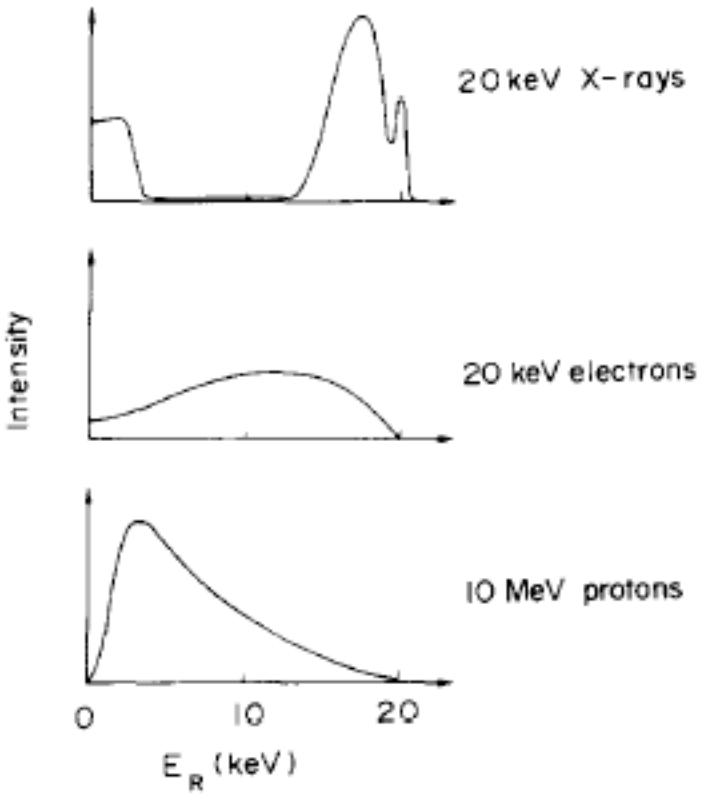

Fig. 7. Background spectra obtained with the three different excitation mechanisms used in X-ray analysis.

How do we focus X Rays?

1. diffraction

2. reflection ("mirrors")

bent xtals

OR

capillary "optics"

internal reflection

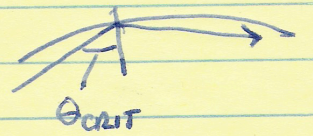

$$\theta_{CRIT} = \frac{\hbar\omega_p}{E_x}$$ ← plasmon energy in material

(glass, $\hbar\omega_p = 30eV$

$\therefore$ if $E_x = 1KeV$

then $\theta_{CRIT} = 30mr$!

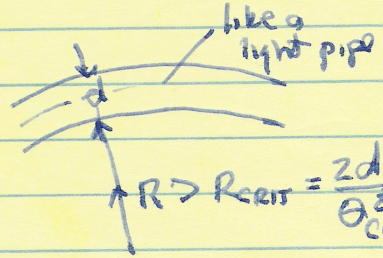

$$R > R_{CRIT} = \frac{2d}{\theta_{CRIT}^2} \Rightarrow \propto E_x^2$$

example: $d = 0.5mm$, $E_x = 1KeV$

gives $R_{CRIT} = 10^2 cm$!

3. ZONE PLATES

How to Detect X Rays?

1. by wavelength (WDS)

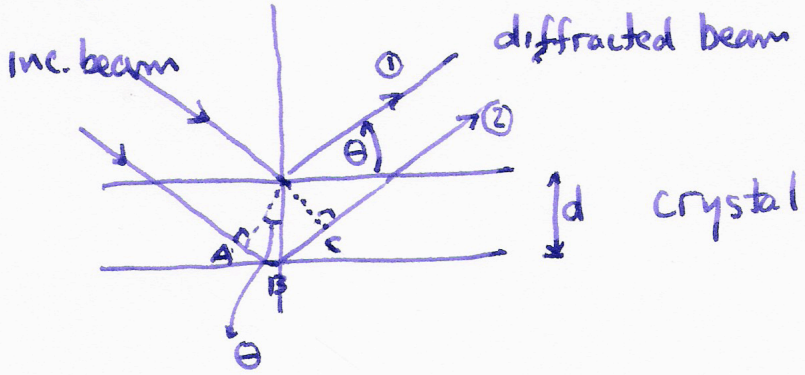

path difference between ① and ② is:

$$\overline{AB} + \overline{BC} = 2d\sin\theta$$

constructive interference between the two beams diffracted (reflected) off the 2 layers is:

path diff $= n\lambda$, $n = 0, 1, 2.$

λ = X-Ray wavelength

$$\therefore \boxed{n\lambda = 2d\sin\theta}$$ Bragg's law → $E = h\nu = \frac{hc}{\lambda}$

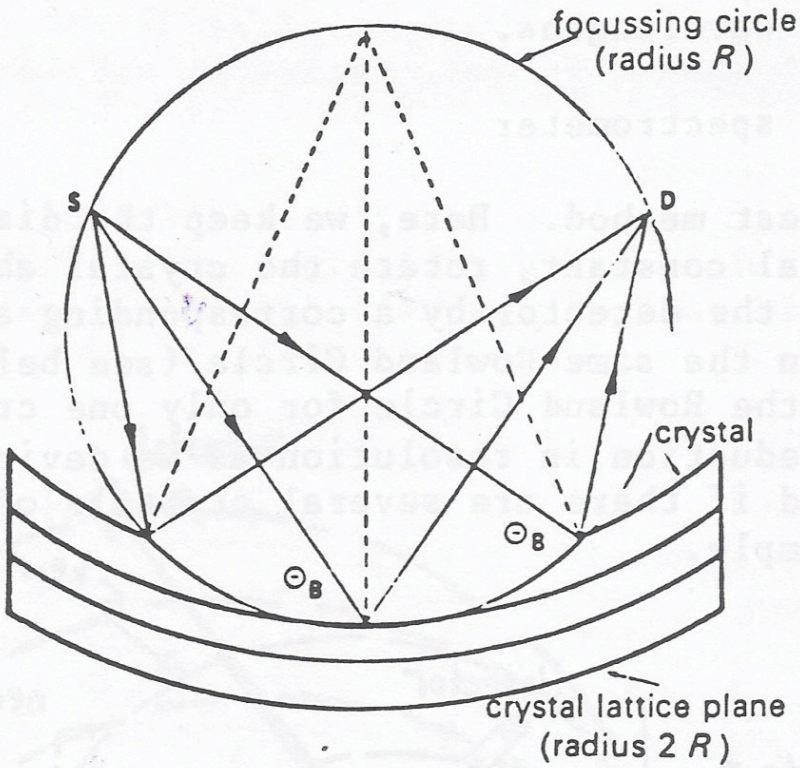

— Johansson mounting.

How do we focus X Rays?

1. diffraction

2. reflection ("mirrors")

bent xtals

OR

capillary "optics"

internal reflection

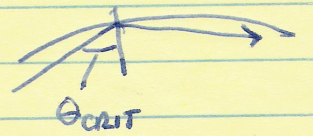

$$\theta_{CRIT} = \frac{\hbar\omega_p}{E_x}$$ ← plasmon energy in material

(glass, $\hbar\omega_p = 30eV$

$\therefore$ if $E_x = 1KeV$

then $\theta_{CRIT} = 30mr$!

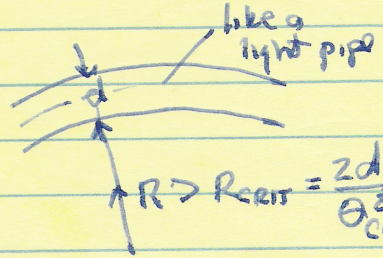

$$R > R_{CRIT} = \frac{2d}{\theta_{CRIT}^2} \Rightarrow \propto E_x^2$$

example: $d = 0.5mm$, $E_x = 1KeV$

gives $R_{CRIT} = 10^2 cm$!

3. ZONE PLATES

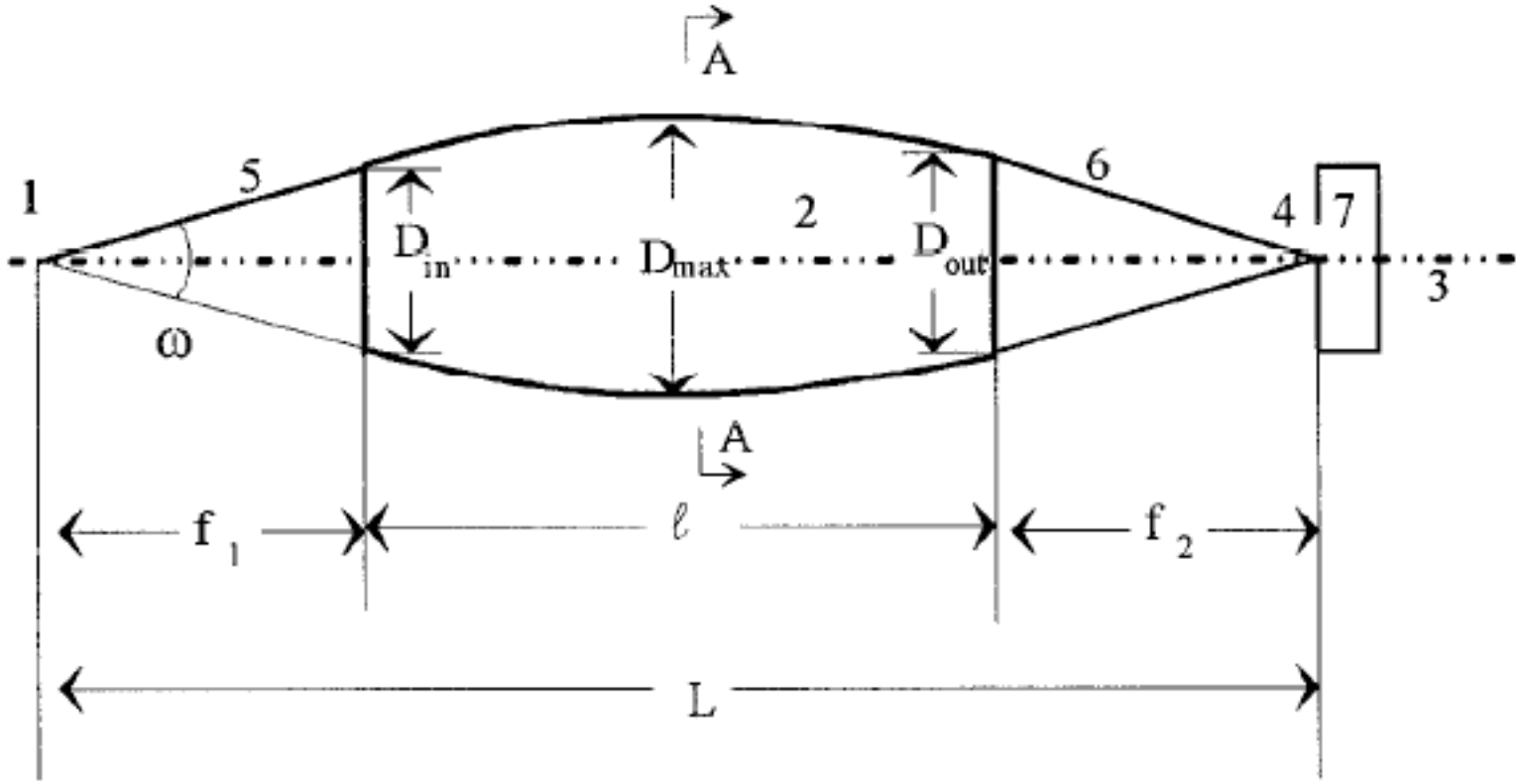

Fig 1. The principal construction of the focusing lens

1 - X-ray source, 2 - lens, 3 - axis of lens, 4 - focal spot,
5 - captured X-rays, 6 - focused X-rays, 7 - X-ray receiver.

From Kumakhov et.al. Phys. Reports. 191(5).1990.pp.289-350.

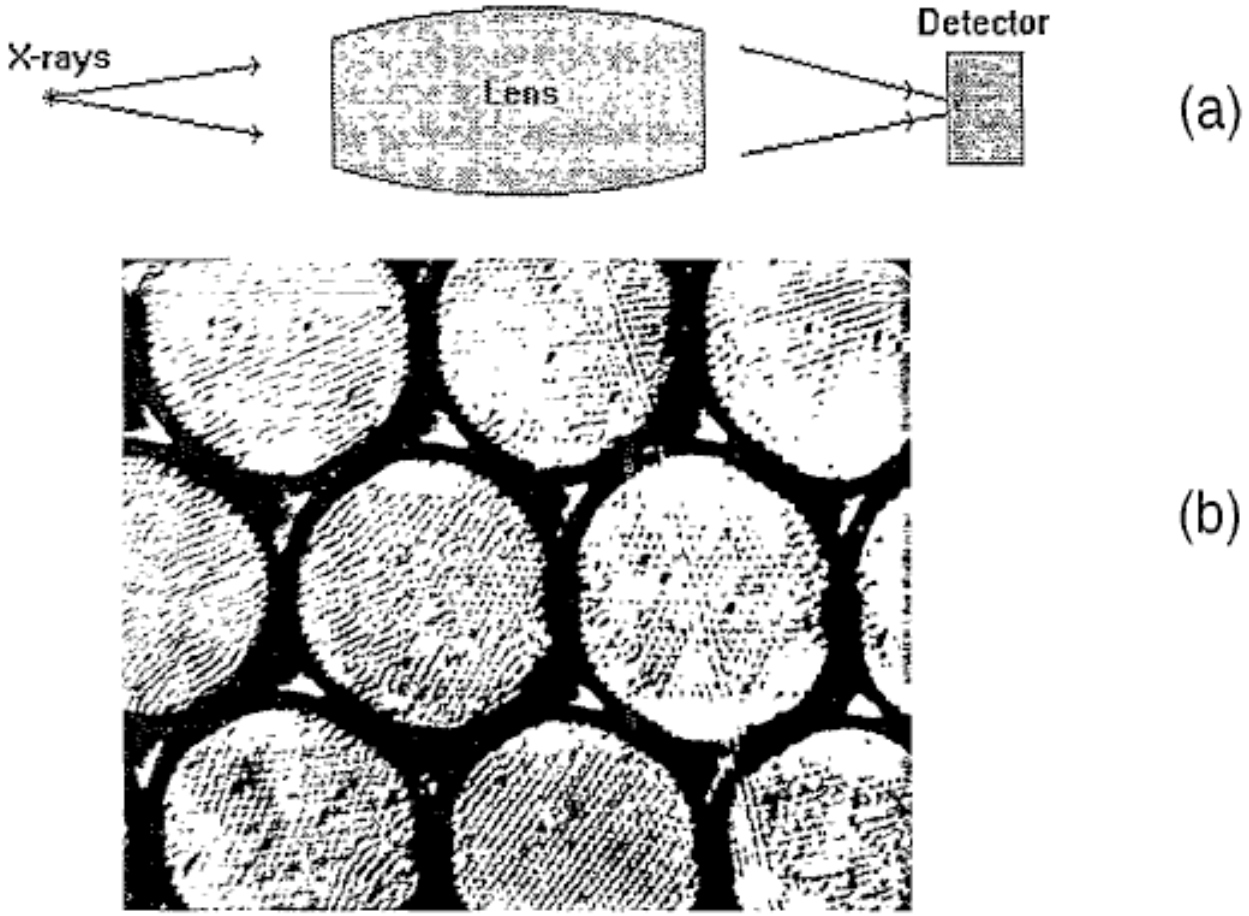

Fig. 1. Scheme of the experiment on focal spot research (a) and close-up photo of the lens end showing the polycapillary structure of the lens (b).

How do we focus X Rays?

slide from before/

1. diffraction

2. reflection ("mirrors")

bent xtals
OR
capillary "optics"
internal reflection

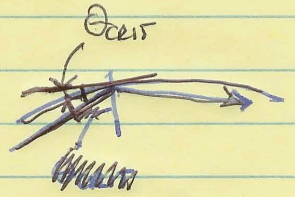

$$\theta_{CRIT} = \frac{\hbar\omega_p}{E_x}$$

← plasmon energy in material

(glass, $\hbar\omega_p = 30eV$

$\therefore$ if $E_x = 1KeV$
then $\theta_{CRIT} = 30mr$!

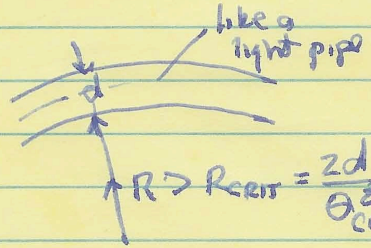

$$R > R_{CRIT} = \frac{2d}{\theta_{CRIT}^2} \Rightarrow \propto E_x^2$$

example: $d = 0.5mm$, $E_x = 1KeV$
gives $R_{CRIT} = 10^2 cm$!

3. ZONE PLATES

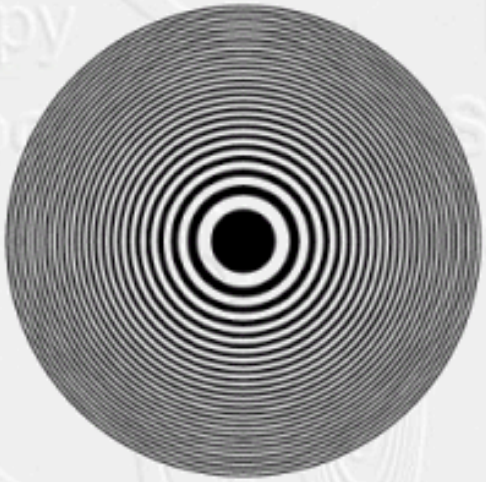

Schematic of a Fresnel zone plate

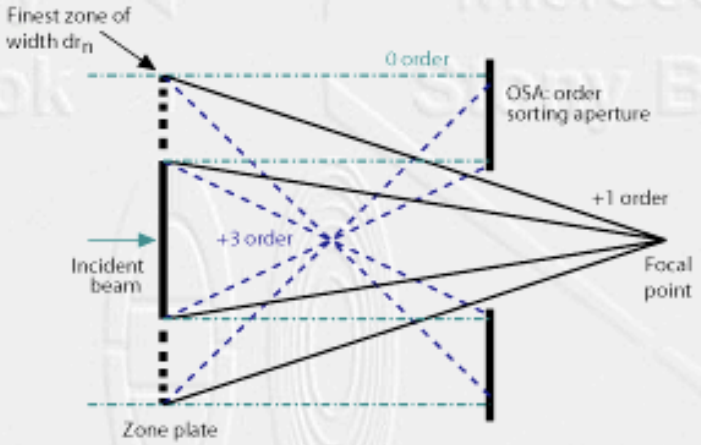

Combination of a central stop and an order-sorting aperture (OSA) to isolate the first-order focus

Area of rings are the same. Get interference between adjacent zones. Get multiple order interference. For xrays, you need to have the “transparent” regions be thin low Z material and the “opaque” regions be thick high Z material to get reasonable efficiency.

ZONE PLATES

(Fresnel lenses)

resolution (spot size), $r = 1.22\,\Delta R_N$

where ΔR_N = width of outermost zone

focal length $f = \dfrac{2 R_N \Delta R_N}{\lambda}$

R_N = radius outer zone

$$r = \frac{0.61 f \lambda}{R_N}$$

NOTE: this is for 1st order interference.
there are higher order focus spots!

need to block out

Note that resolution gets better the larger the ring and the smaller the ring width.

TYPES OF XRAY MICROSCOPES

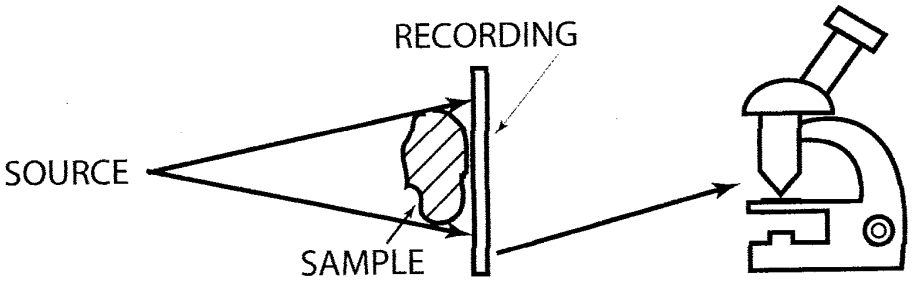

A

CONTACT MICROSCOPE

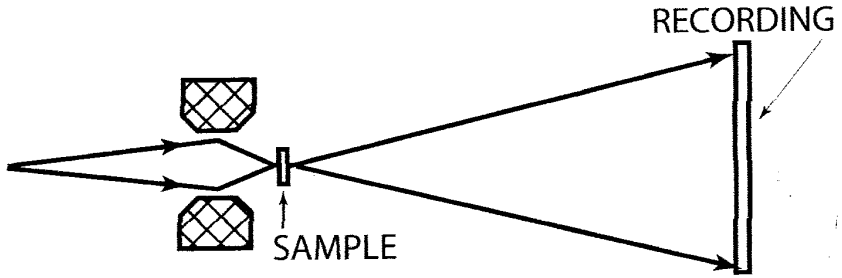

B

PROJECTION MICROSCOPE

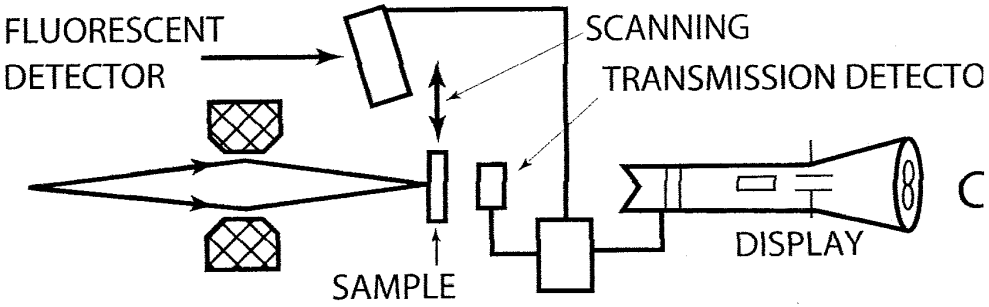

C

SCANNING MICROSCOPE

X Ray Microscopes

look at different methods for x Ray Microscopy

doc cam

1. contact Microscope
   use absorption $I(t) = I_0 e^{-\int_0^t \mu(x)dx}$

depends on source size

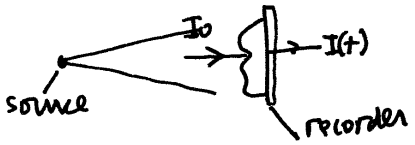

— measure integrated absorption
— record for diff. λ

2. projection Microscope (a lensless method)
   (Roentgen) 1895.
   similar principle.
   — resolution limited by:
      1. source size.
      2. Fresnel diffraction
      3. penumbra effect

doc cam pix

3. scanning Microscope
   1. mechanical scanning of sample
   2. scanning of source.

→ good review/ J. Kirz. J Phys. Conf. Ser. 186(2009) 012001.
9th Int Conf. on X Ray Microscopy / history and future

PROJECTION MICROSCOPY

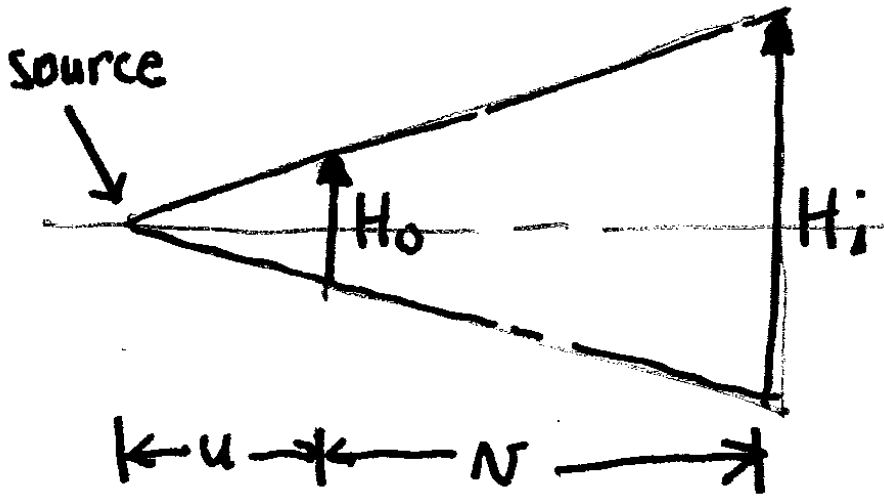

$$\frac{H_i}{u+v} = \frac{H_o}{u}$$

$$\frac{H_i}{H_o} = \frac{u+v}{u} = 1+\frac{v}{u}$$

$$\frac{H_i}{H_o} \cong \frac{v}{u} \quad \text{if } v \gg u$$

$\frac{H_i}{H_o}$ → the "magnification"

Projection X Ray Microscopy

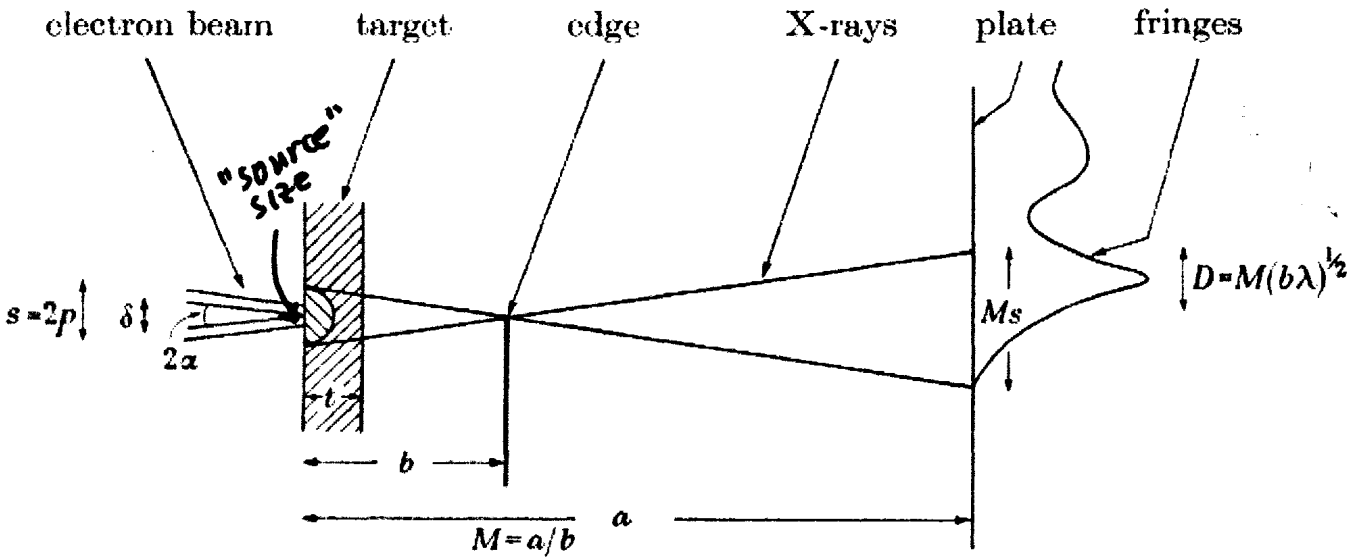

FIGURE 1. Image formation by projection microradiography. Unsharpness in image plane $= Ms$. First Fresnel fringe half-width in image plane $= M(b\lambda)^{\frac{1}{2}}$.

From: W. Nixon. Proc. Roy. Soc. Lond. A (1955).

S.C. Mayo, et al. J. Microscopy. 207. Pt 2. (2002). 79-96.

Hand mit Ringen: print of Wilhelm Röntgen's first "medical" x-ray, of his wife's hand, taken on 22 December 1895 and presented to Professor Ludwig Zehnder of the Physik Institut, University of Freiburg, on 1 January 1896[4][5]

Xray Microscopy

Detected “species”

- transmitted xrays
- emitted xrays (fluorescence)
- emitted electrons (photo electric effect)

Xray Photoemission Microscopy

Introduction

Photoelectric effect

Photoelectric effect

Einstein, Nobel Prize 1921

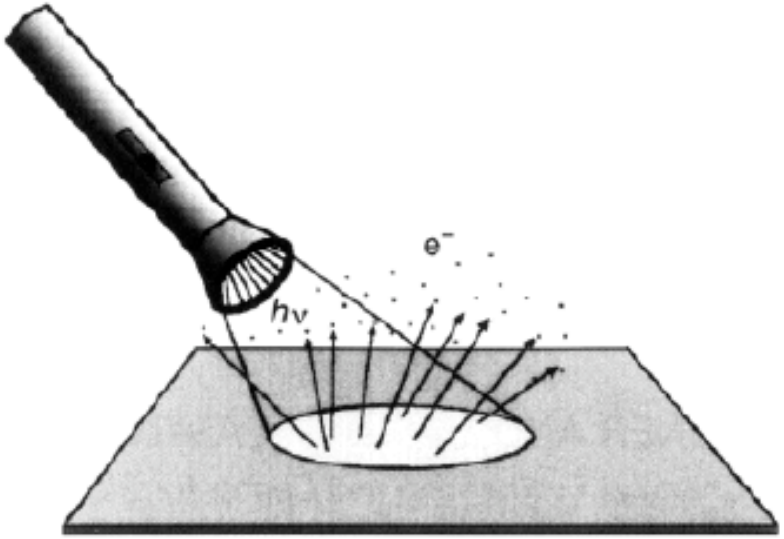

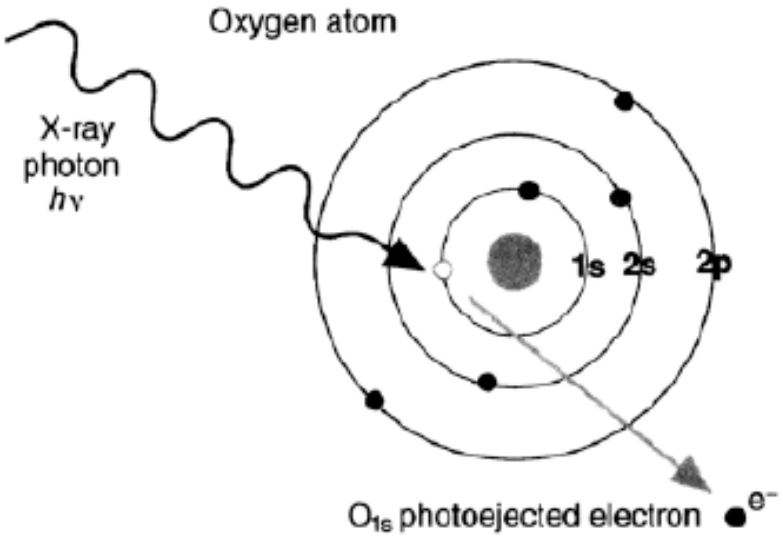

Photoemission as an analytical tool

Kai Siegbahn, Nobel Prize 1981

$E_{max} = hf - E_b$

From Smart, et.al. U.Western Ontario

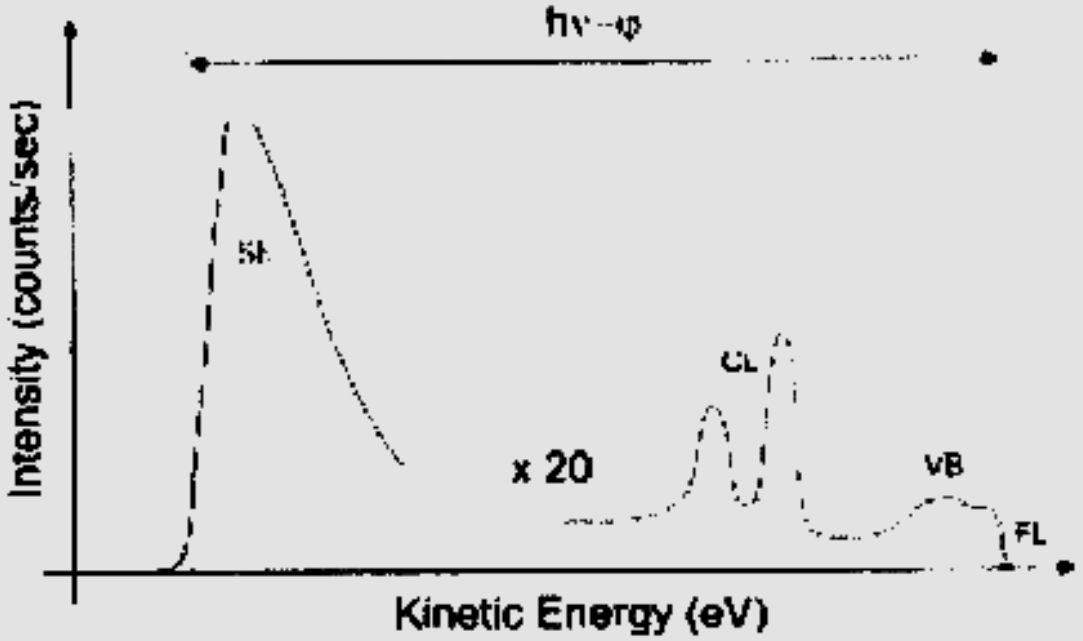

Fig. 1. Typical PE emission spectrum. SE: secondary electrons, CL: core level, VB: valence bond, FL: Fermi level, $h\nu$: photon energy, ϕ: work function of the specimen.

EE213 Lect # 11

How do we get an "XPS" image?

show slides

1. focus xrays and "scan" them
2. focus xrays and "scan" sample
3. image photoelectrons emitted with a lens
   - electrostatic lens —
     have large aberrations —
     particularly Cc
     remember, generally using medium energy X rays
   - electrons from sample ~1keV or less.
     and they aren't completely monochromatic
     for resolutions $\ll 1\,\mu m$ need aberration corrections
     very complex — correct with a "mirror"
     - symmetric — equal/opposite inversions

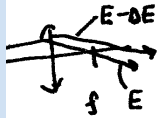

mentions
ectrode
lempfer —

4. use scanning e beam to produce Xrays?
   what resolution do you expect?

ref. E. Bauer. J. Phys. Cond. Matter. 13(49) 2001. p11391.
photoelectron Microscopy

S. Gunther, et. al. Prog in Surf. Sci. 70(2002). 187-260.

from Janos Kirz, '09

nitride windows [47].

- The first undulator beamline for microscopy at the NSLS [48].
- The establishment of the Center for X-ray Optics in Berkeley by David Attwood.
- Spectromicroscopy using XANES [31, 49, 50, 51, 52].

Most of these conference proceedings are relatively easy to come by [53, 54, 55, 56, 57, 58]. The proceedings of the Sep. 20–24, 1993 conference held in Chernogolovka, Russia are a bit harder to find [59], but the conference was memorable: the Congress of People's Deputies was dissolved by President Boris Yeltsin on Sep. 21, and rumors were rampant during the meeting. Most foreign participants had returned home before street riots and battles took place over Sep. 28-Oct. 5.

1.6. The Age of Reason 1994–2002

X-ray microscopy started a major expansion during this period, with new instruments at new light sources, such as ALS, APS, ESRF, ELETTRA, NSRRC, Spring-8, Aarhus, Ritsumeikan, etc. Tomography [60, 61], cryo [62, 63], and cryo-tomography [64, 65, 66, 67] were demonstrated. The range of applications grew rapidly, including soil science, geochemistry, polymer science, magnetism, etc. Groups in Göttingen, Stockholm, London, Tsukuba and elsewhere were designing and building laboratory-based instruments. David Sayre's old dream of di raction microscopy (recording the di raction pattern of a non-crystal, and reconstructing it) had its first successful realization at the NSLS [68].

1.7. The Industrial Revolution 2003–2008

In the last five years X-ray microscopy has entered the mainstream. We are no longer working with an esoteric, new, unproven technique. What brought about this change is the rapidly growing list of successful and highly visible applications in environmental and soil science, geo- and cosmo-chemistry, polymer science, biology, magnetism, energy research, materials and surface science, among others. Without applications we are just a curiosity.

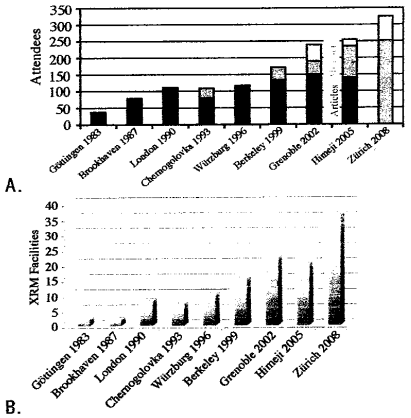

Figure 6. Growth in the x-ray microscopy community. A) Number of attendees, articles with abstracts, and abstracts only at the modern series of x-ray microscopy conferences. The number of articles at the 2008 meeting is not indicated in this figure. B) X-ray microscopy facilities at synchrotron light sources worldwide. The count is based on papers presented at each x-ray microscopy conference.

what are issues in producing a small table top x-ray source?

1. finely ~~focuse~~ focussed electron "spot" / how small?
2. high current in spot
3. good conversion efficiency ($e^- \rightarrow$ x-rays)

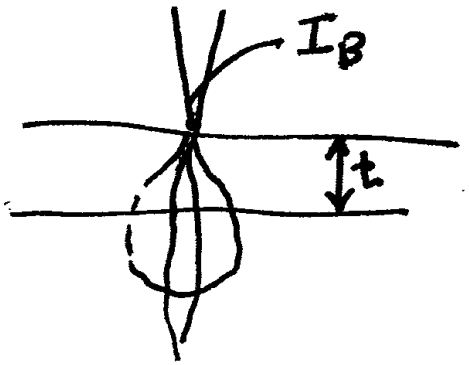

EE 213 Lecture #11 — Photoelectron spectroscopy I

$S = NJ\sigma\gamma F$

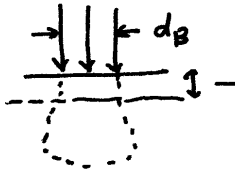

— probed volume — thickness ~ $3\times\Lambda_{esc}$

for Auger:

we had $S(WXY) = [n\lambda I_p(1+R^*)]\,\sigma(E_i,E_p)\,\gamma(WXY)\,[r_R^* T]$

(NJ = $[n\lambda I_p(1+R^*)]$; Y = $\gamma(WXY)$; F = $[r_R^* T]$)

$\lambda \rightarrow \int_0^\infty dt\, e^{-t/\lambda}$ — attenuation on the way out

for X rays in, we get something similar:

1) $n\sigma(1+R^*)$ — X rays not backscattered

2) $\sigma\omega \rightarrow \sigma_{ij}$ the X ray absorption cross section for a particular binding energy to result in ejected photo elec

3) $I_p \rightarrow$ # X rays/sec impinging

4) n = # atoms/volume — same

5) λ = escape depth a IMFP / same.

6) F = detector/analyzer efficiency

∴ for X rays: $S_i = n_i \lambda_i \sigma_i F_i I_p$ → this is Smart's K //

NOTES on IMFP//

Inelastic MFP

$$\sigma_{IN} \cong \frac{35.7\sqrt{Z}}{E_p} \ln\left(\frac{4E_p}{12.3\sqrt{Z}}\right) \text{ in } \text{Å}^2 \text{ if } E_p \text{ in eV} \;/\; \text{Inner energies}$$

$$\lambda_{esc} \cong \lambda_{IN} = \frac{1}{n_z \sigma_{IN}}$$

$$\overline{E}_{loss} \cong 12.3\sqrt{Z} \text{ eV}$$

$$\therefore \boxed{\lambda_{esc} \cong \frac{E_p}{35.7\, n_z \sqrt{Z} \ln(4E_p/12.3\sqrt{Z})}} \text{ in Å}$$

NOTE: $n_z\sqrt{Z}$ ↗ slightly with Z ($.24, Z=6 \rightarrow .52, Z=79$)

but $\ln(4E_p/12.3\sqrt{Z})$ ↘

so λ_{esc} NOT TOO material dep.

Seah & Dench
J. Surf. Interf. Anal. 1, 36 (1979)

least squares fit to data (10^2–10^4 eV)

$$\boxed{\lambda_{esc} \cong .057\sqrt{E_p}} \text{ in Å, } E_p \text{ in eV}$$

the 2 expressions differ by abt 10–20%

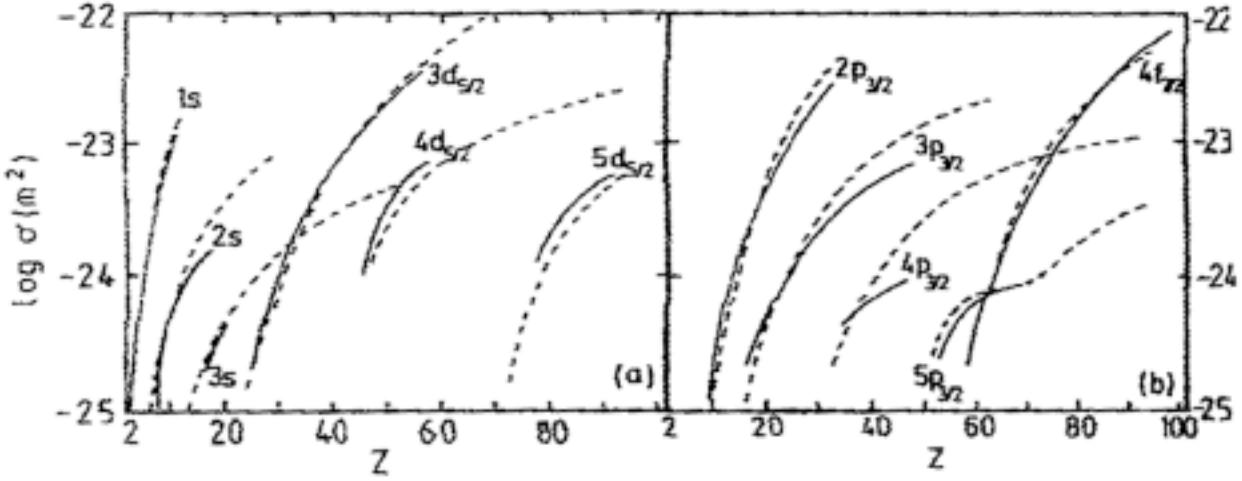

Fig.26. Photoionization cross-sections of the atomic levels as a
of atomic number at an excitation energy hν = 1.5 keV.
values apply not only to Aℓ K_α (hν = 1487 eV) but appr
also to Mg Kα (hν = 1254 eV) (adapted from ref.52). Dashe
theoretical values, solid lines: adjusted experimental valu

Other sources for X Ray Microscopy

Bibliography of Soft X-ray Microscopy - REFERENCES

Originally published as supplemental material for

H. Ade and A.P. Hitchcock, *NEXAFS microscopy and resonant scattering: Composition and orientation probed in real and reciprocal space,* Polymer 49 (2008) 643-67

A.P. Hitchcock

File: XRM-bib-ref.doc Last changed: 05-Jan-2012 (aph)

CODE: YYYYABC or **YYYYAB&** where YYYY = year , A – first letter of last name of first author, B – first letter of last name of second author, C – first letter of last name of third author; if more than 3 authors, replace C with &; if not unique, append a, b, c etc

CONFERENCE PROCEEDINGS

1st Int. Conf. X-ray Microscopy	Göttingen, Germany	1983 G. Schmahl, and D. Rudolph (Eds) **X-ray microscopy** (Springer, 1984)
2nd Int. Conf. X-ray Microscopy	Stony Brook, USA	1987 D. Sayre, M. Howells, J. Kirz, H. Rarback (Eds.) **X-Ray Microscopy II** (Springer, 1988)
3rd Int. Conf. X-ray Microscopy	London, UK	1990 A. Michette, G. R. Morrison, and C. J. Buckley (Eds.) **X-Ray Microscopy III** (Springer, 1992)
4th Int. Conf. X-ray Microscopy	Chernogolovka, Russia	1993 V. V. Aristov, and A. I. Erko (Eds.) **X-Ray Microscopy IV** (Chernogolovka, Russia, 1994).
5th Int. Conf. X-ray Microscopy	Würzburg, Germany	1996 J. Thieme, G. Schmahl, D. Rudolf, E. Umbach (Eds) **X-ray microscopy and spectromicroscopy** (Springer, 1998)
6th Int. Conf. X-ray Microscopy	Berkeley, USA 1999	W. Meyer-Ilse, T. Warwick, and D. Attwood (Eds.) **Am. Inst. Phys. Conf. Proc 507** (2000)
7th Int. Conf. X-ray Microscopy	Grenoble, France	2002 J. Susini, D. Joteux, F. Polack (Eds) **J. de Physique IV Proceedings 104** (2003)
8th Int. Conf. X-ray Microscopy	Himeji, Japan	2005 S. Aoki, Y. Kagoshima, Y. Suzuki (Eds) **IPAP Conference Series 7, Proc. 8th Int. Conf. on X-ray Microscopy**
9th Int. Conf. X-ray Microscopy	Zurich, Switzerland	2008 Christoph Quitmann, Franz Pfeiffer (eds) **J. Physics: Conference Series: Proc. 9th Int. Conf. on X-ray Microscopy Vol 186** (2009)
10th Int. Conf. X-ray Microscopy	Chigaco, USA	2010 Ian McNulty, Catherine Eyberger, Barry Lai (eds) **Am. Inst. Phys. Conf. Proc. 1365** (2011)
11th Int. Conf. X-ray Microscopy	Shanghai, China	2012 Ziyu Wu, Renzhong Tai (eds)

ESRF, Grenoble

History of Photoelectron Microscopy

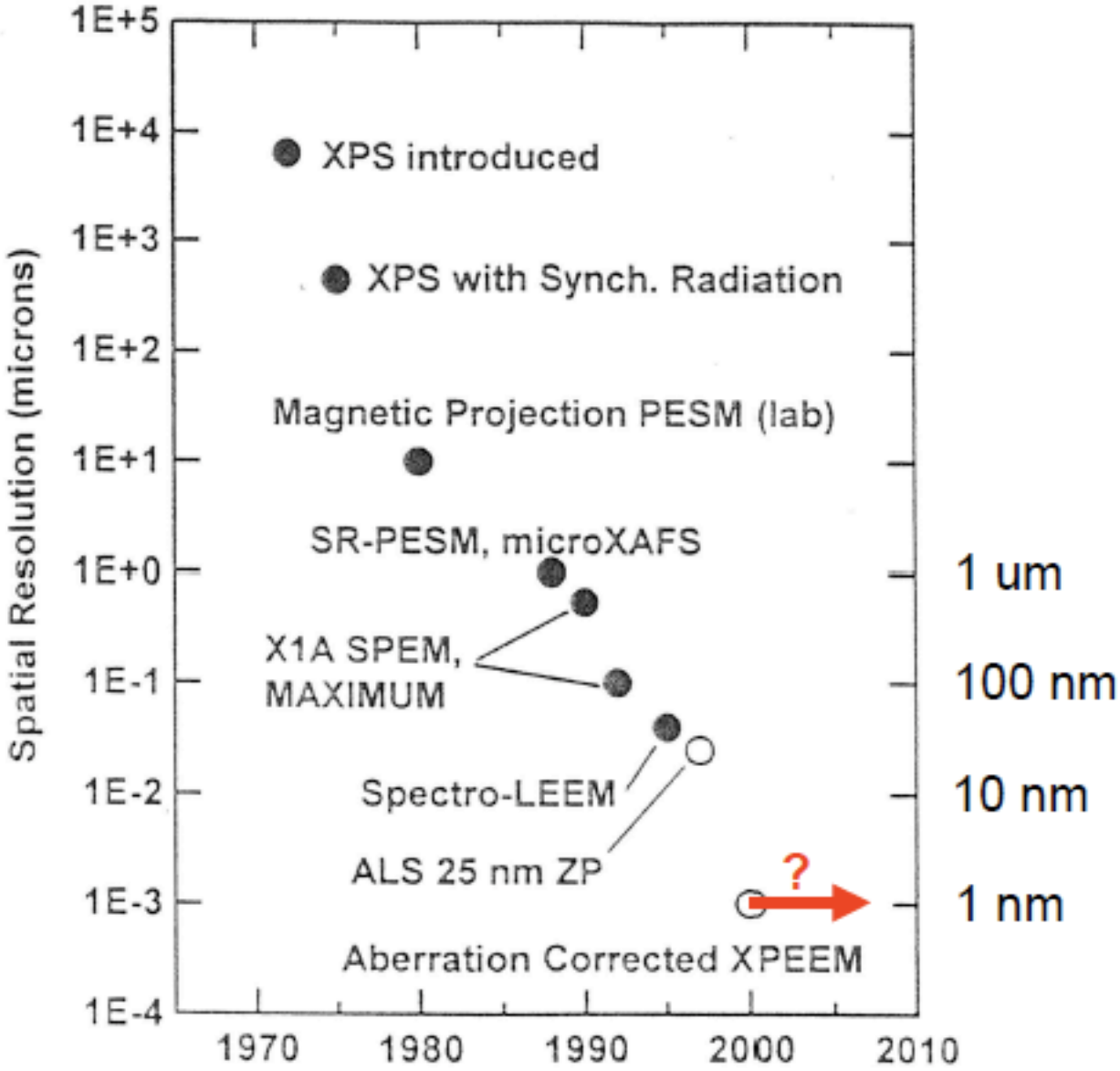

From S. Heun Tutorial, CNR-INFM, Trieste

Table Top Xray Microscopes

9th International Conference on X-Ray Microscopy
Journal of Physics: Conference Series **186** (2009) 012010

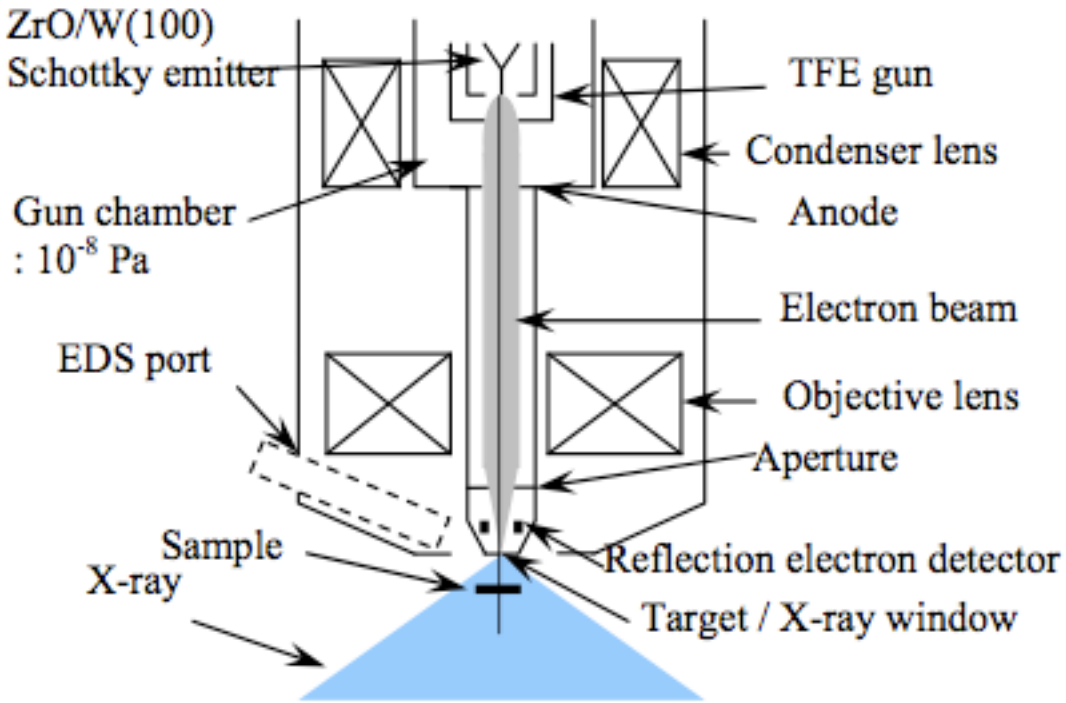

Figure 1. Schematics of nano-focus X-ray tube "TX-510".

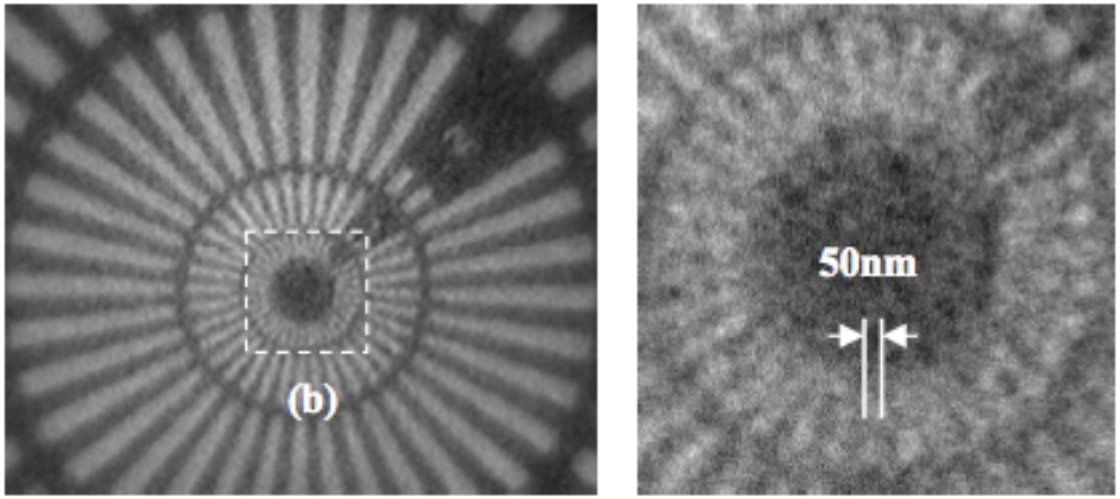

(a) (b)

Figure 4. X-ray images of X-ray resolution test chart taken by using TUX-5000FS. A low magnification image (a). The minimum width of radial line and space of the inner circle is 50nm in digital magnified image (b). Accelerating voltage is 30kV and emission current from TFE gun is 160μA. Target material is platinum of 0.6 μm thick.

Products

Advanced product development and innovative research greatly depends on effective imaging solutions to expose internal structures and allow researchers and engineers to develop and confirm models to describe the properties and behavior of materials of interest. Key to effective imaging is the ability to use a succession of increasing resolutions combined with smaller and smaller fields of view to allow you to 'zoom' into the particular area of interest. Ideally you can start with scanning mode, using a large field of view up to centimeters in size and resolution of tens of microns. You then move on to resolutions in the sub micron scale with a field of view of a few millimeters, and further down to nanoscale resolution with a field of view of microns. In addition, as product and sample complexity increases, it becomes more and more challenging to fully understand the three dimensional intricacies of structures, so that 3D imaging modalities are required. Alternative two dimensional imaging modalities such as TEM and FIB/SEM require complex procedures and skills to reconstruct the 3D models and confirm three dimensional dependencies between the various internal structures of the sample.

VersaXRM-500

MicroXCT-200

MicroXCT-400

UltraXRM-L200

Xradia offers X-ray microscopes (XRM), advanced imaging solutions using X-ray computed tomography (CT) scanning technology combined with proprietary X-ray optics. Xradia's multi-lengthscale solution combines the VersaXRM family and UltraXRM lab platforms to provide the only 3D non-destructive imaging solution from millimeter to nanometer length scale. The VersaXRM utilizes patented X-ray detectors and an optical microscope style turret with magnifying objective detectors for easy zooming. You can go from a scanning mode and about 30 micron resolution all the way down to sub-micron pixel resolution with about 2 mm field of view. The UltraXRM nanoscale X-ray microscope is the only commercially available X-ray microscope that utilizes synchrotron based X-ray optics and provides true sub-100 nm 3D volumetric resolution.

The MicroXCT platform includes the following systems –

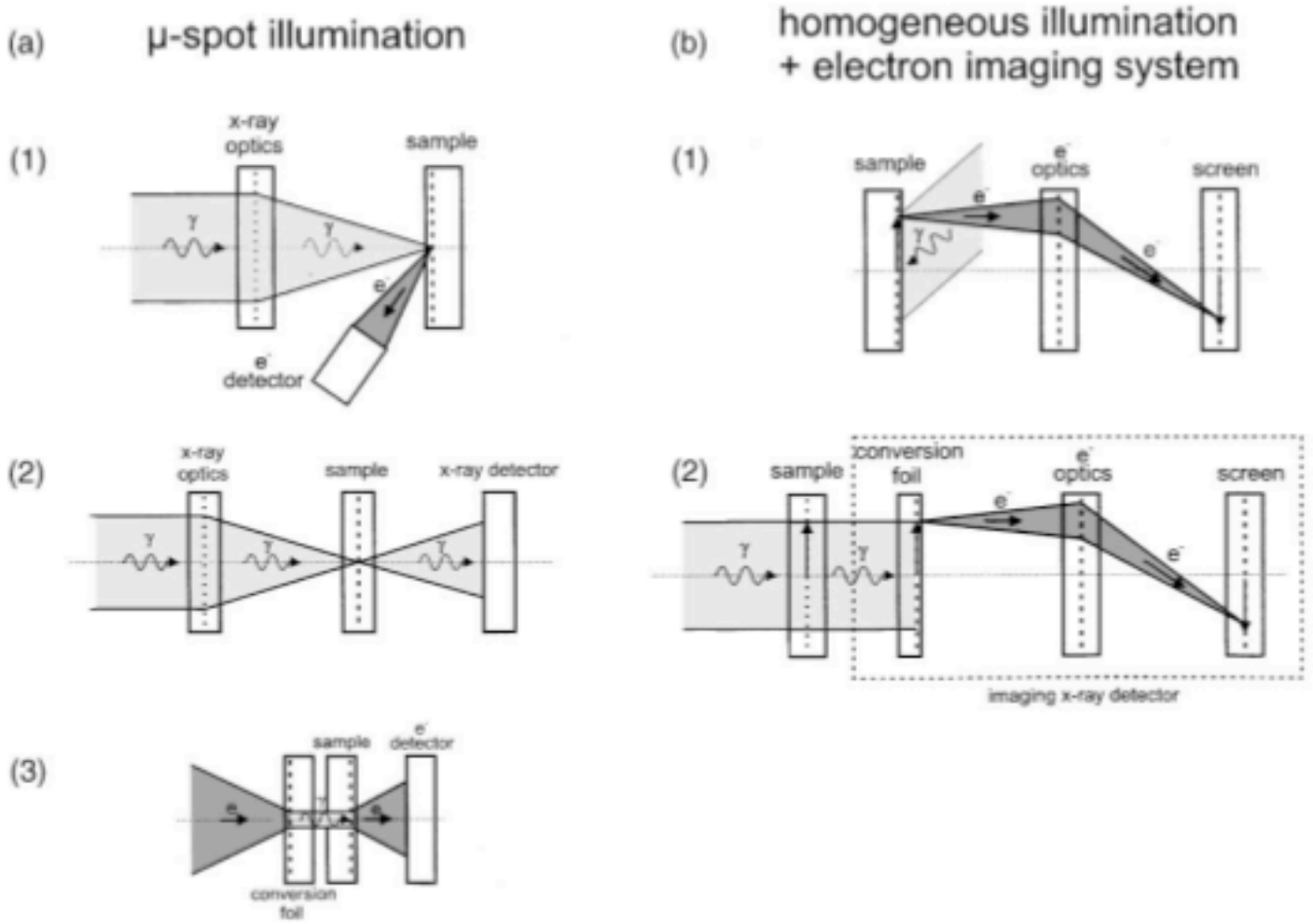

Fig. 5. Schematic illustration of used source–sample–detector geometries in PEM: (a) μ-spot illumination in scanning instruments, (b) electron imaging systems. The present review focuses on systems using geometry 1. Geometries 2 and 3 are listed for sake of completeness (see text).

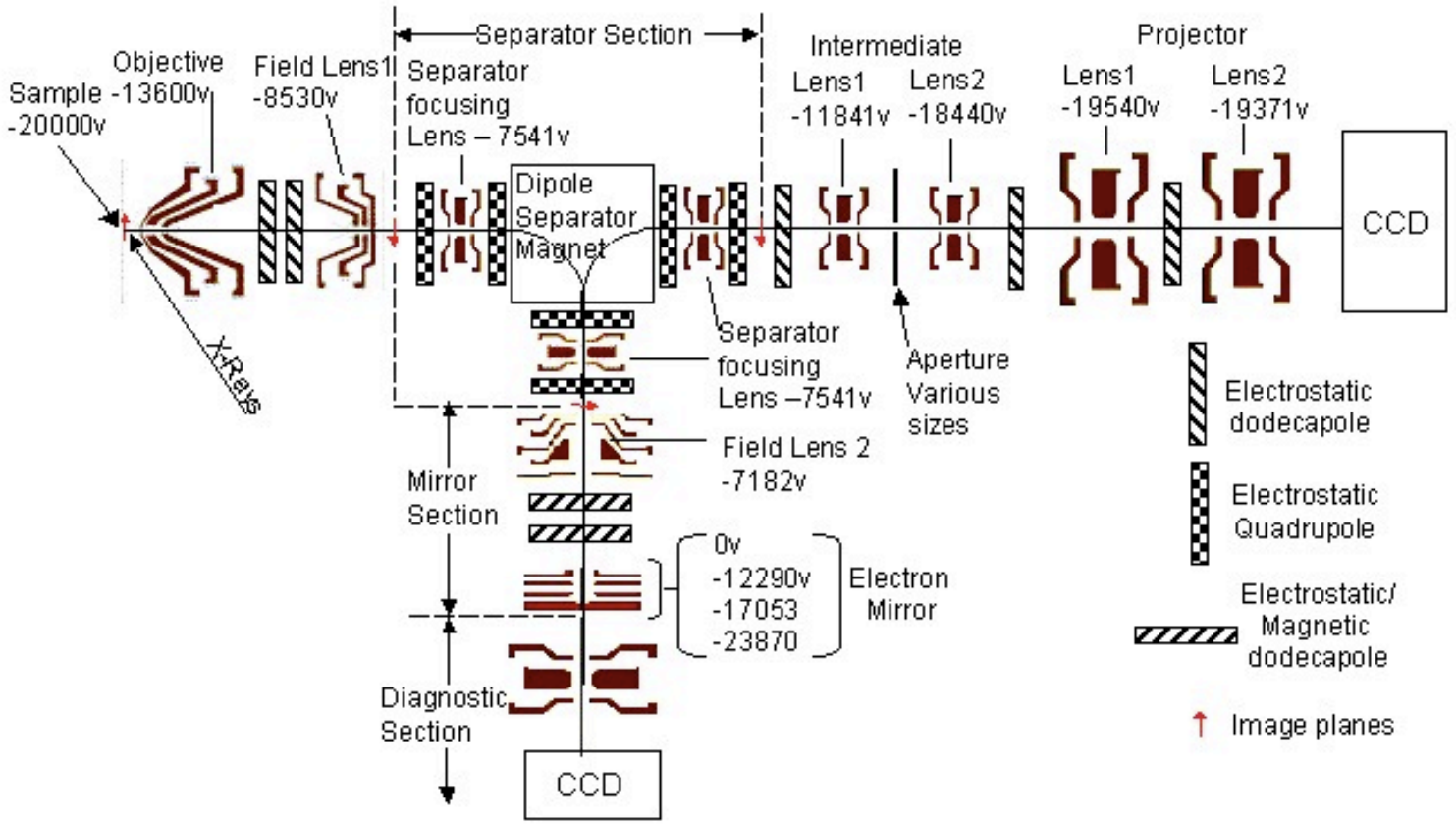

The aberration corrected microscope PEEM-3 employs a curved electron mirror to counter the lowest order aberrations of the electron lenses and the accelerating field.A dipole separator magnet directs the electron beam into the mirror and back into the projector optics of the microscope. Four mirror electrodes allows us to fine-tune spherical and chromatic aberration correction and magnification (-1) of the mirror. Backfocal plane apertures between 10 μm and 50 μm can be chosen to optimize resolution and transmission. A three-lens projector optics produce a total optical magnification between 300 and 10000. Electrostatic and magnetic deflectors are used for beam-stearing and shaping.

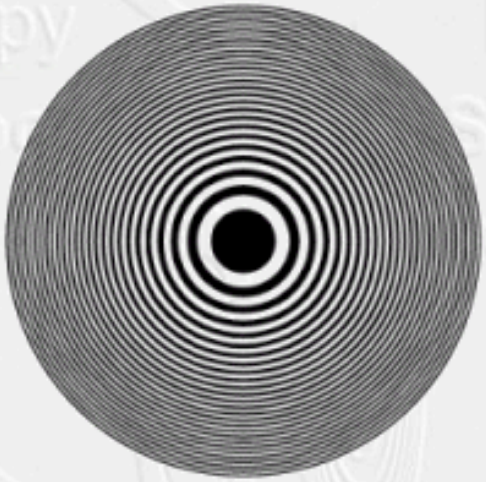

Schematic of a Fresnel zone plate

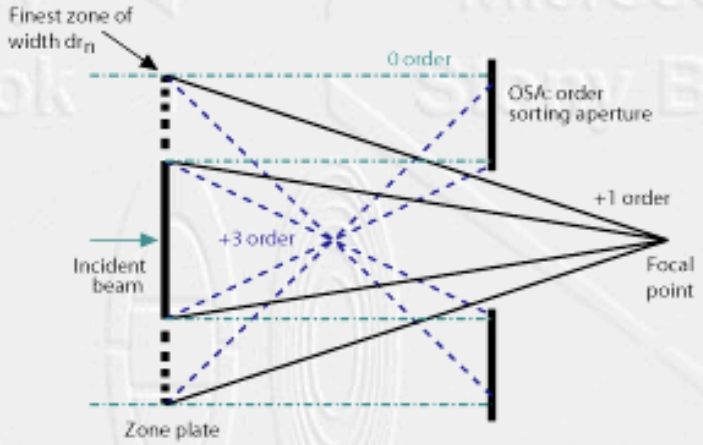

Combination of a central stop and an order-sorting aperture (OSA) to isolate the first-order focus

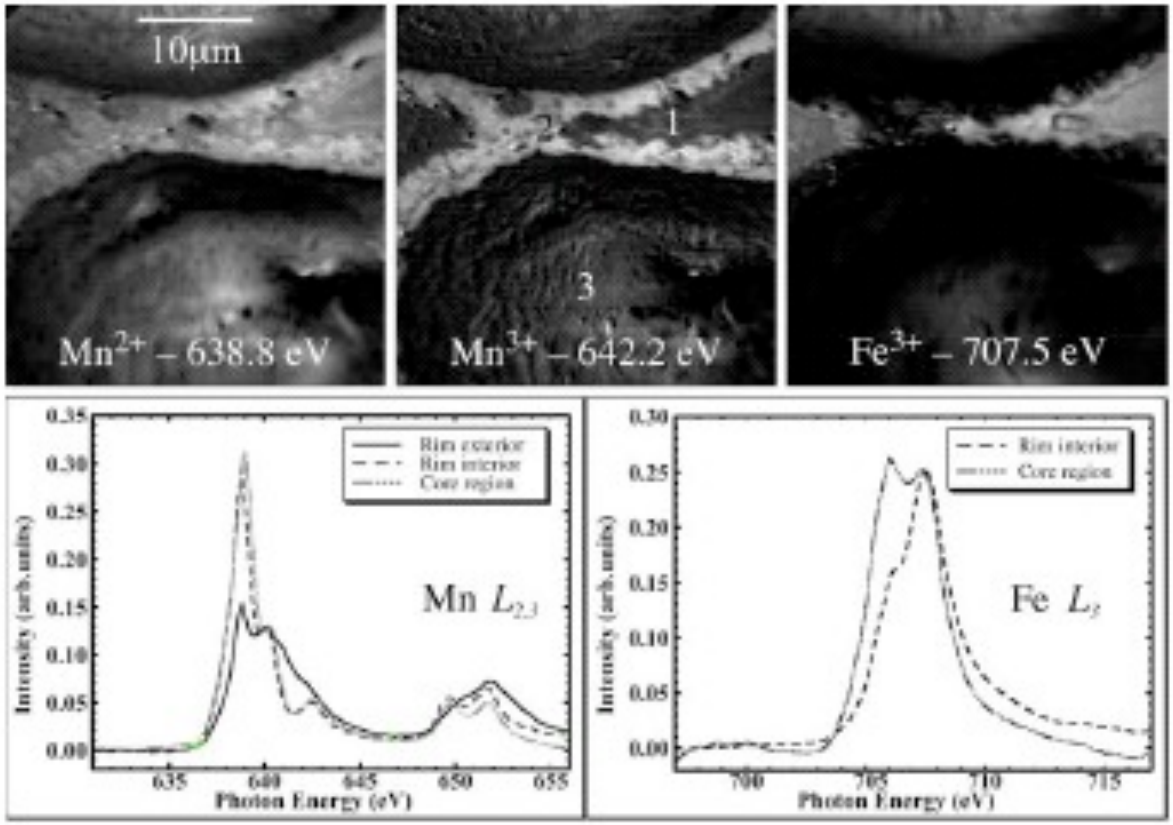
10μm
1
2
3
Mn^{2+} – 638.8 eV
Mn^{3+} – 642.2 eV
Fe^{3+} – 707.5 eV
Rim exterior
Rim interior
Core region
Mn $L_{2,3}$
Intensity (arb. units)
Photon Energy (eV)
Rim interior
Core region
Fe L_3
Intensity (arb. units)
Photon Energy (eV)

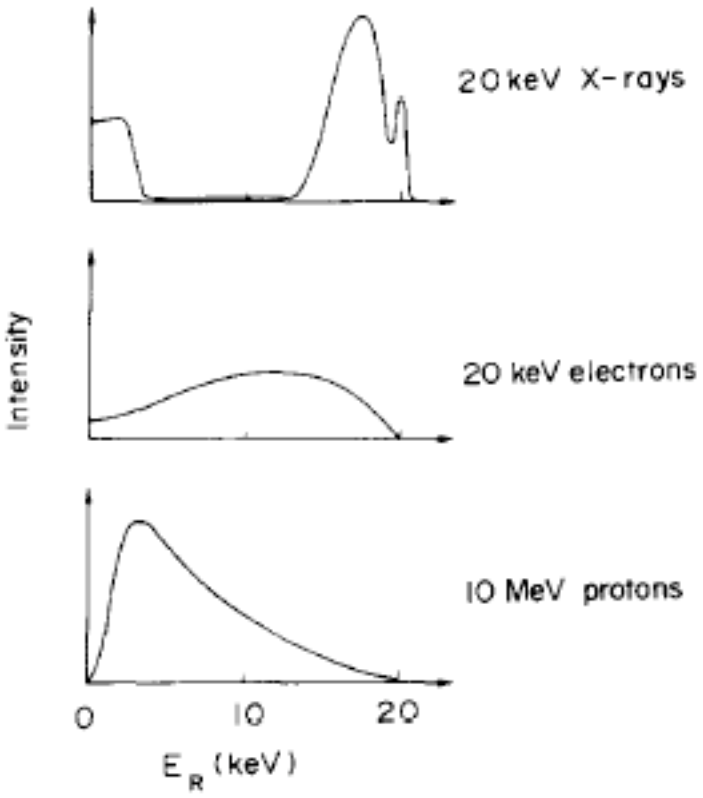

Fig. 7. Background spectra obtained with the three different excitation mechanisms used in X-ray analysis.

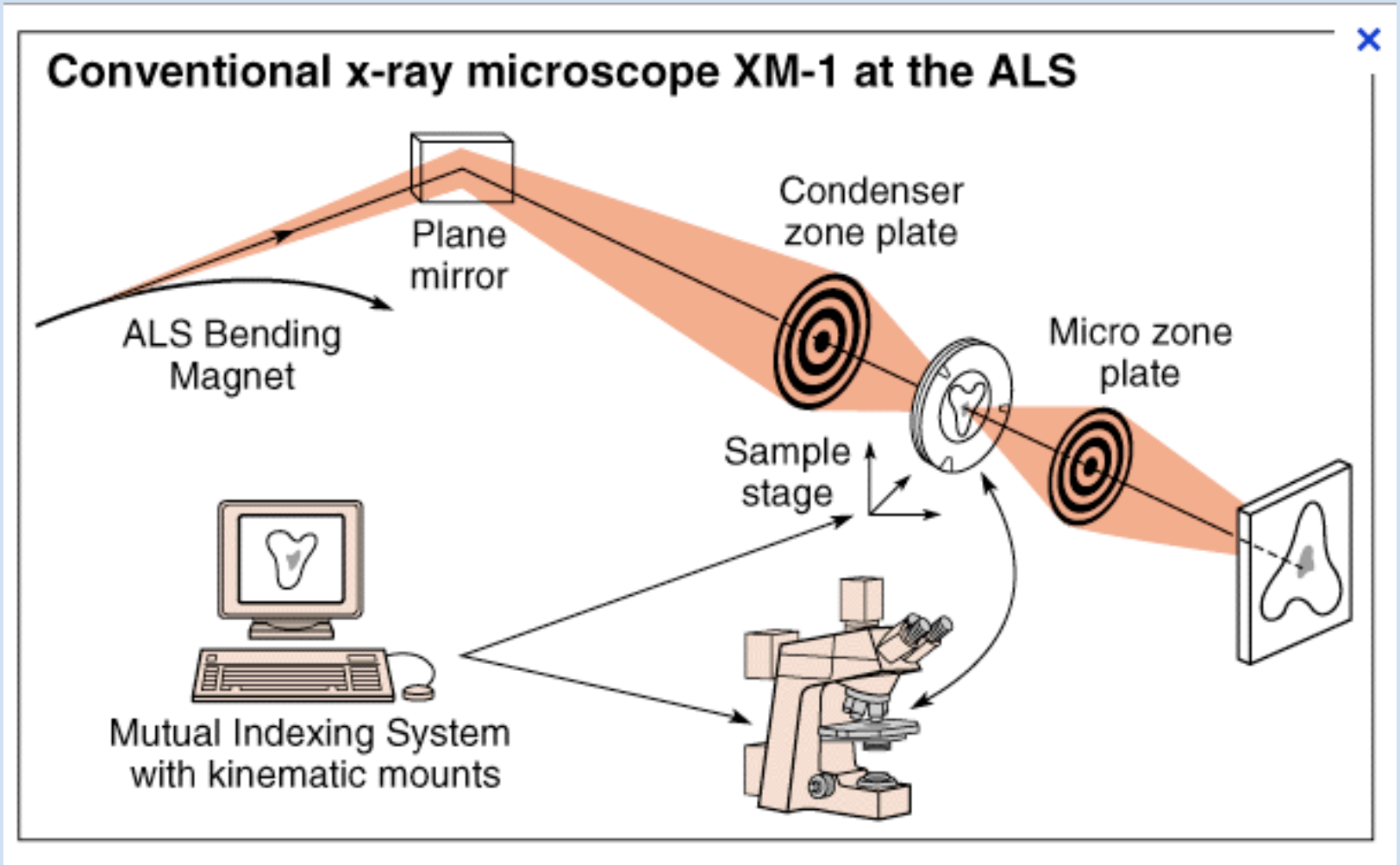
Conventional x-ray microscope XM-1 at the ALS
Plane mirror
Condenser zone plate
ALS Bending Magnet
Micro zone plate
Sample stage
Mutual Indexing System with kinematic mounts

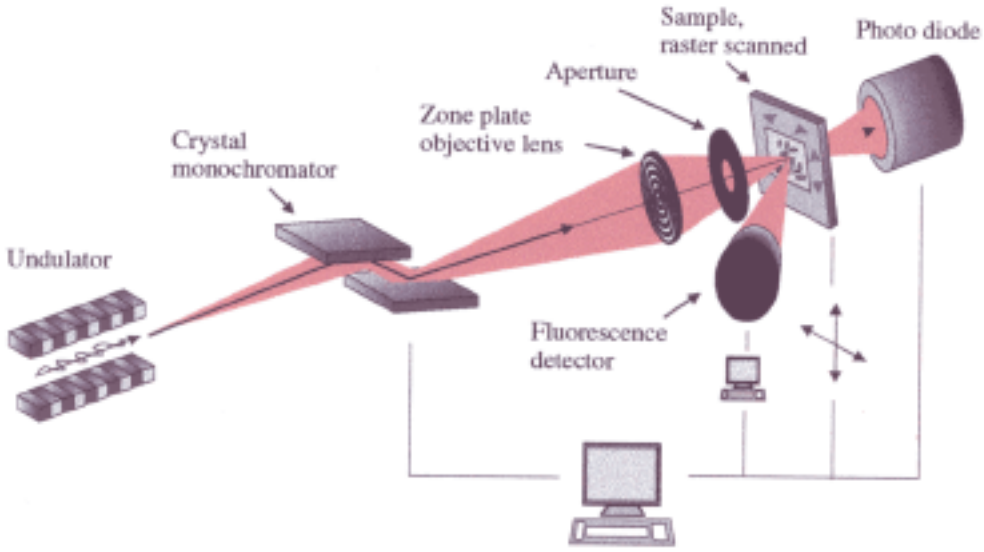

Fig. 2. Schematic of the scanning X-ray microscope.

At ESRF (European Synchrotron Radiation Facility, Grenoble)

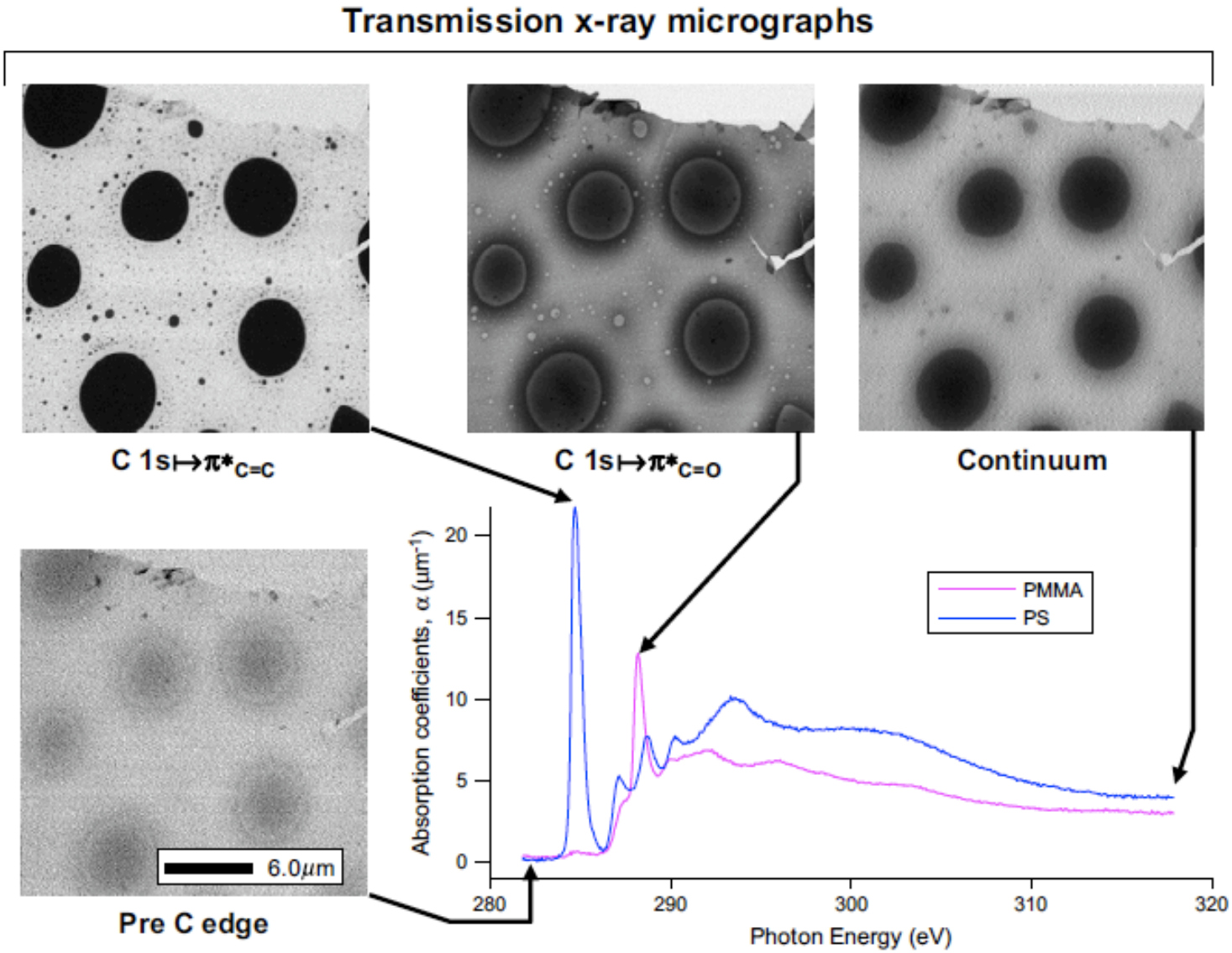

Fig. 13. Transmission images of a simple, binary PS and PMMA thin film blend, annealed on a SiO_x substrate such that large droplets have formed. Reference spectra of PS and PMMA are shown, along with the images that correspond to the characteristic energies as indicated. The complete morphology cannot be inferred from an individual image.

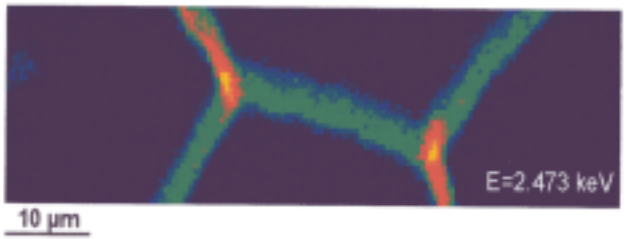

(a)

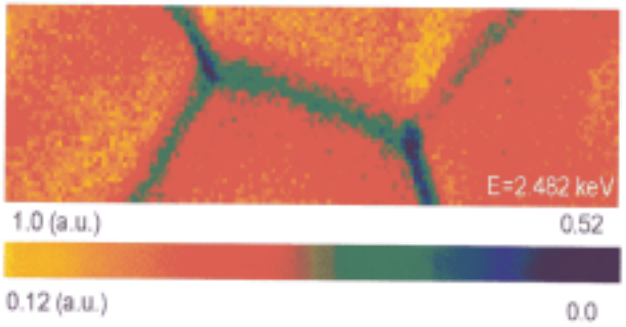

(b)

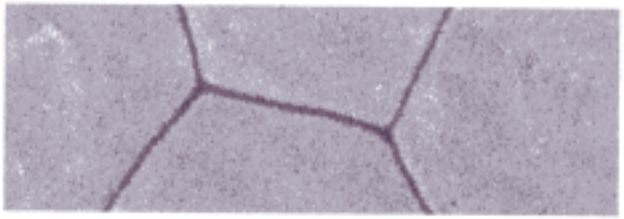

(c)

Fig. 5. Fluorescence yield images of a *Pinna* shell taken at two energies, 2.473 keV (a) and 2.482 keV (b), specific of the sulfur in sulfate or amino acid forms respectively. The pixel size is $0.5 \times 0.5\ \mu m^2$. An electron microscope image is given for comparison (c).

435|30 June 2005|doi:10.1038/nature03719

19.5 nm half-period

15.1 nm half period

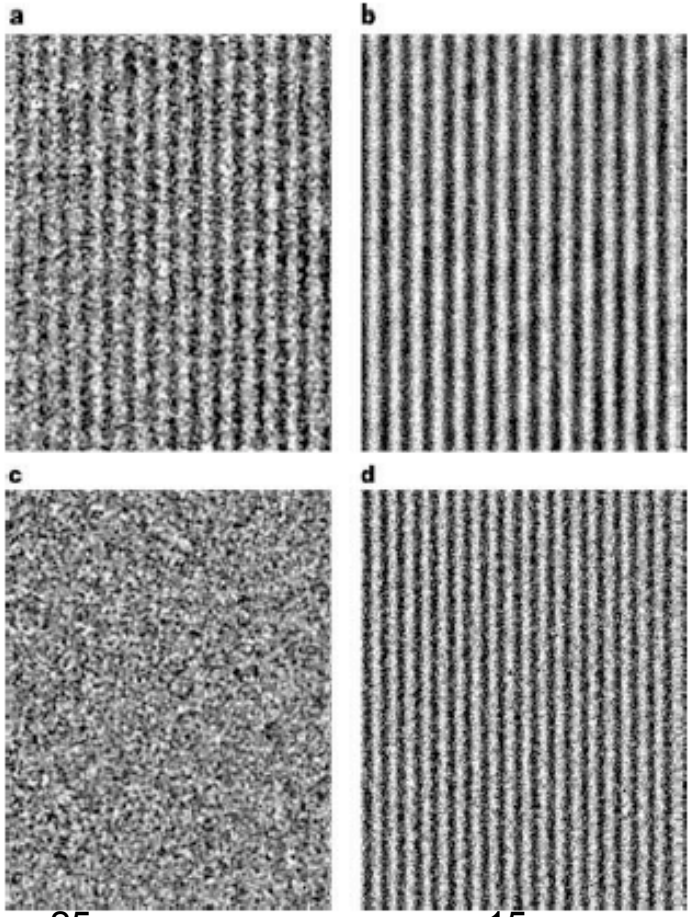

25 nm 15nm ---------- width of outer ring of zone plate

Figure 4 | Soft X-ray images of 15.1 nm and 19.5 nm half-period test objects, as formed with zone plates having outer zone widths of 25 nm and 15 nm. The test objects consist of Cr/Si multilayers, with 15.1 nm and 19.5 nm half-periods, respectively. Significant improvements are noted between the images obtained with the new 15 nm zone plate, as compared to earlier results obtained with the 25 nm zone plate. This is particularly evident for the 15 nm half-period images, for which the earlier result shows no modulation, whereas the image obtained with the 15 nm zone plate shows excellent modulation. **a**, Image of 19.5 nm half-period test object obtained previously with a 25 nm zone plate. **b**, Image of 19.5 nm half-period object with the 15 nm zone plate. **c**, Image of 15.1 nm half-period with the previous 25 nm zone plate. **d**, Image of 15.1 nm half-period with the 15 nm zone plate. Images **a** and **c** were obtained at a wavelength of 2.07 nm (600 eV photon energy); **b** and **d** were obtained at a wavelength of 1.52 nm (815 eV). The equivalent object plane pixel size for images **a** and **c** is 4.3 nm; the size for **b** and **d** is 1.6 nm.